Modeling Equilibrium Dynamics of the Benguela Current System

JENNIFER VEITCH

Department of Oceanography, University of Cape Town, Rondebosch, South Africa

PIERRICK PENVEN

Laboratoire de Physique des Oceans (UMR 6523 CNRS, IFREMER, IRD, UBO), Brest, France

FRANK SHILLINGTON

Department of Oceanography, University of Cape Town, Rondebosch, South Africa

(Manuscript received 14 October 2009, in final form 12 February 2010)

ABSTRACT

The Regional Ocean Modeling System (ROMS) is used to systematically investigate equilibrium conditions and seasonal variations of the Benguela system at a resolution of 9 km, including both the large-scale offshore flow regime and the economically and ecologically important coastal upwelling regime. A shelf-edge poleward flow exists in the northern Benguela region (i.e., north of ~28°S) and is driven primarily by the wind stress curl via the Sverdrup relation. As such, it is strongly seasonal and is most intense during spring and summer, when the wind stress curl is most negative. The poleward flow deepens as it moves southward; between ~25° and 27°S, much of it veers offshore because of the nature of the wind stress curl and its interaction with the northwestward path of the Benguela Current, which is influenced by alongshore topographical variations. The Benguela Current is driven by nonlinear interactions of passing Agulhas rings and eddies and does not have a striking seasonal signal. In the mean state, it is characterized by two streams. The more inshore stream is topographically controlled and follows the run of the shelf edge. The meandering nature of the offshore stream is a result of the preferential path of Agulhas rings. The model simulates all seven of the major upwelling cells within its domain. The three southernmost cells have the strongest seasonal signal and experience their greatest upwelling during spring and summer months, whereas the two northernmost cells have less seasonal variability but nevertheless have increased upwelling from autumn to spring (and least upwelling in summer), and the central Benguela upwelling cells experience year-round upwelling. The effect of topography on coastal upwelling was investigated by smoothing alongshore coastline and topography variations, which showed that, in all of the seven major upwelling cells, upwelling is enhanced on the downstream side of capes.

1. Introduction

The Benguela system is the eastern boundary current system of the South Atlantic Ocean and is situated off the west coast of southern Africa (for its geographic location and a schematic of the salient features, refer to Fig. 1). As one of the world's four major eastern boundary upwelling systems, the geographical location of the Benguela system is unique in that its southern boundary is coincident with the termination of both the African continent as well as the warm-water regime of the western boundary current of the Indian Ocean (the Agulhas Current). In this work, the Benguela system is defined as both the nearshore upwelling area and its associated shelf-circulation features as well as the large-scale Benguela Current (BC). We define the Benguela Current as the eastern limb of the South Atlantic subtropical gyre (STG) and the cool nearshore water simply as the Benguela upwelling regime.

In this work, the Benguela upwelling regime is defined as the cool coastal region extending northward from the southern tip of Africa to ~14°–16°S. Upwelling in the Benguela system is controlled by the anticyclonic winds of the South Atlantic Anticyclone (SAA), which are guided by the thermal barrier setup by the coastline of

Corresponding author address: Jennifer Veitch, Department of Oceanography, University of Cape Town, Private Bag X3, Rondebosch 7701, South Africa.
E-mail: jennifer.veitch@uct.ac.za

DOI: 10.1175/2010JPO4382.1

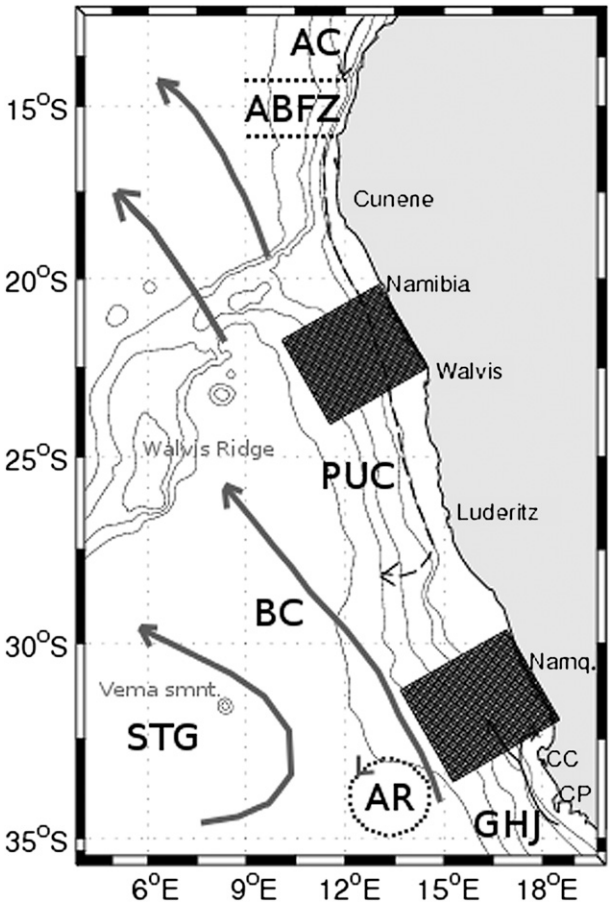

FIG. 1. A schematic representation of the Benguela system. The gray contours show the 300-, 500-, 1000-, 3000-, and 4000-m isobaths: note the location of the Walvis Ridge and the Vema Seamount. Locations of the seven major upwelling cells are labeled. Some important features are shown: AC, ABFZ, PUC, BC (thick gray arrows), AR, GHJ, and STG (the outer limb of which contributes to the BC: refer to the text for expansions of the features.). The two gridded boxes indicate regions characteristic of the northern and southern Benguela regimes.

the subcontinent, giving rise to the alongshore equatorward winds on the west coast of Africa (Nelson and Hutchings 1983). The seasonal shift of the SAA along a northwestward axis (Preston-Whyte and Tyson 1993) gives rise to seasonal variations of upwelling along the southwest African coast. Although upwelling exists all along the west coast of southern Africa, seven centers of enhanced upwelling have been identified (e.g., Nelson and Hutchings 1983; Lutjeharms and Meeuwis 1987); the locations of these centers have been associated with areas of locally enhanced wind stress curl and a change of coastline orientation (Shannon and Nelson 1996). A modeling study allowed Veitch et al. (2008) to explicitly reveal the disparate northern and southern Benguela systems. Their model revealed all of the seven upwelling cells as well as their seasonal variation. The Lüderitz upwelling cell at ~27.5°S is the most vigorous and separates the more perennial upwelling region in the north (with a slight maximum during winter) from the strongly seasonal upwelling signal of the southern Benguela (which experiences peak upwelling in summer). The seaward extent of coastal upwelling is demarcated by a convoluted thermal front that has different characteristics in the northern and southern parts of the system. South of Lüderitz, the upwelling front is well defined and tends to follow the shelf edge, whereas it is more diffuse in the north (Shannon and Nelson 1996).

The Benguela Current lies offshore of the Benguela upwelling area and has been defined as the eastern boundary current of the anticyclonic South Atlantic subtropical gyre (Peterson and Stramma 1991). Transport of the Benguela Current is supplied by the southern limb of the South Atlantic subtropical gyre, by south Indian Ocean waters via the Agulhas Current, and can be influenced by Subantarctic Surface Water via perturbations in the Subtropical Front. In fact, geostrophic transports derived from observational data by Gordon et al. (1987) suggest that as much as 10 Sv (1 Sv $\equiv 10^6$ m^3 s^{-1}) of a total flow of 15 Sv into the upper 1500 m of the South Atlantic is fed by the Agulhas Current, with the rest (5 Sv) being fed by the South Atlantic Current.

The northern boundary of the Benguela upwelling area is commensurate with the Angola–Benguela frontal zone (ABFZ), which has been defined as the confluence between the cool Benguela upwelling regime and the warm Angola Current (AC). It presents a cross-frontal dichotomy in water masses (Mohrholz et al. 2001) and in biological distribution and abundance (John et al. 2001). The ABFZ is situated between ~15° and 17°S and is oriented in a west to northwesterly direction from the coast (Shannon et al. 1987). Using high-resolution satellite sea surface temperature (SST) data, Veitch et al. (2006) observed that the surface expression of the front was widest (narrowest) with most (least) intense gradients in summer (winter). The seasonal cycle of the intensity of the ABFZ has been related to fluctuations of upwelling-favorable wind stress, whereas its north–south migration is related to changes in the poleward flow associated with its northern boundary that in turn is related to the curl of the wind stress (Colberg and Reason 2006). The significance of the ABFZ on the Benguela upwelling regime lies principally in the fact that it presents a gateway into the ecologically sensitive upwelling system for water of equatorial–tropical Atlantic origin.

The southern boundary of the Benguela system abuts the retroflection area of the Agulhas Current that has been extensively described and investigated by Lutjeharms

and van Ballegooyen (1988) and Gordon (2003), among others. The importance of the retroflection lies in its role in the Indian–Atlantic Ocean exchange of heat and salt and thus is also thought to have a key role in the maintenance of the global overturning of the ocean (Gordon et al. 1992; Lutjeharms 1996). The primary mechanism of heat and salt exchange is via Agulhas rings (AR) or eddies that shed at the Agulhas retroflection, merge with the Benguela Current, and travel into the Atlantic. The shedding of eddies at the Agulhas retroflection therefore has a significant control on the nature of the Benguela Current near its source. In fact, Matano and Beier (2003) found that much of the energy of the Benguela Current originates from Agulhas eddy fluxes. Boebel et al. (2003) coined the term Cape Cauldron to describe the regime of turbulent mixing in the Cape Basin offshore of the southern Benguela upwelling system that is a consequence of the path and interaction of anticyclonic Agulhas eddies as well as smaller cyclonic eddies that are formed within the Cape Basin.

Understanding of the dynamics of the California Current system (e.g., Marchesiello et al. 2003), as well as the Peru Current system (e.g., Penven et al. 2005), has improved considerably because of the advancement of modeling capabilities so that simulations encompassing the whole system can be run at sufficiently high resolutions to capture salient features of upwelling dynamics. Though some model-based research has been carried out in the Benguela system, they have either not encompassed the whole system (Penven et al. 2001, 2000; Blanke et al. 2005) or have focused on basin-scale features and have therefore been run at low resolution (Skogen 1999; Lutjeharms et al. 1995). In this two-part work, we characterize salient features of the Benguela system in a cohesive manner using a numerical model that is inclusive of the whole system at a high resolution. In this paper, we focus on equilibrium dynamics of the Benguela Current and upwelling regime and aim to clarify the present understanding of the mean state and seasonal cycle of these aspects of the system. A thorough understanding of the seasonal variability of the system is essential if we are to improve our chances of predicting extreme events. A follow-up will investigate the role of mesoscale variability in the Benguela system.

The layout of the paper is as follows: section 2 describes the model simulation and configuration as well as the satellite and in situ data sources used for comparisons. For an idea of the success of the simulation, model output is compared with satellite and in situ data in section 3a. This is followed by a description and analysis of model results for the large-scale flow regime and for the coastal upwelling regime in section 3b. Possible topographical control of both the large-scale regime and upwelling rates are investigated in section 3c. Section 4 provides a discussion and synthesis of this work.

2. Methods

a. ROMS

A high-resolution (~9 km), nested configuration of the Regional Ocean Modeling System (ROMS) is used to simulate the seasonal dynamics of the Benguela system. ROMS is a split-explicit, free-surface, topographic-following coordinate model that is well suited to regional problems (Shchepetkin and McWilliams 2003, 2005). It solves the incompressible primitive equations based on the Boussinesq and hydrostatic approximations and is coupled with advection/diffusion schemes for potential temperature and salinity and as well as a nonlinear equation of state. The advection scheme is third-order upstream biased, which reduces dispersion errors, essentially enhancing precision for a given grid resolution (Shchepetkin and McWilliams 1998). The recent implementation of higher-order diffusive advection schemes has lead to spurious diapycnal mixing in sigma-coordinate models. A solution to this problem was addressed by Marchesiello et al. (2009) and involves the split of advection and diffusion, the latter of which appears as a biharmonic operator. This solution was implemented in our nested simulation to preserve the low dispersion and diffusivity capabilities of the original scheme while conserving water mass characteristics.

Lateral viscosity is zero everywhere except in sponge layers at open boundaries, where it increases smoothly toward the edge of the domain. Open-boundary conditions are a combination of outward radiation and nudging toward prescribed external boundary conditions and are described by Marchesiello et al. (2001). Subgrid-scale vertical mixing is introduced by the nonlocal K-profile parameterization (KPP) scheme (Large et al. 1994). The bottom boundary layer is generated by a KPP bottom boundary layer parameterization and a quadratic bottom drag. The bottom friction coefficient is calculated through the use of a logarithmic boundary layer formulation with the bottom roughness of 10 cm.

b. Model configuration

To maximize computing efficiency of a high-resolution simulation of the Benguela system, the Adaptive Grid Refinement in Fortran (AGRIF) nesting capability of ROMS is employed (Debreu and Blayo 2008). The nested approach has been evaluated by Penven et al. (2006b) and is designed such that the boundary conditions of a high-resolution "child" domain are supplied by the

lower-resolution ''parent'' domain within which it is embedded. This allows for more consistent boundary conditions of the child domain than can be obtained from, often sparsely populated, in situ data. Our simulation makes use of the recently updated version of the AGRIF package that allows for a two-way nesting procedure, which also allows the child solution to feed into the parent domain. This is done by interpolating the parent boundary data at the end of each child time step and updating at the end of each parent time step (Debreu and Blayo 2008). A major advantage of the two-way nesting approach is that the feedback of the child grid to the parent grid enables more accurate outflow of features from the child to parent than in a one-way nested approach. This is particularly beneficial when modeling the Benguela system resulting from the thoroughfare of large [~(200–300 km) diameter] Agulhas rings in the Cape Basin region.

The topography of the nested configuration was produced with a bilinear interpolation of the 1′ General Bathymetric Chart of the Oceans (GEBCO; available online at http://www.gebco.net) product. In a further attempt at avoiding pressure gradient errors, the topography has been smoothed to maintain a ''slope parameter'' $[r = (h_{i+1} - h_{i-1})/(h_{i+1} + h_{i-1})]$ of <0.2 (for a more complete description of the method, see Penven et al. 2007). The topographies of the child and parent domains are smoothly connected with a relation that uses an α parameter that is 0 within 15 grids of the child boundaries and reaches 1 as it approaches the lateral boundaries (Penven et al. 2006b).

Because of the focus on equilibrium dynamics and seasonal variability, a 0.5° Quick Scatterometer (QuikSCAT) climatology of 2000–07 wind data was used to force the nested configuration, whereas surface heat and salt fluxes are provided by Comprehensive Ocean–Atmosphere Data Set (COADS) climatologies (Da Silva et al. 1994). The model is initialized from a state of no flow and mean January temperatures and salinities from the *World Ocean Atlas 2005* (*WOA05*; Conkright et al. 2002). The absence of an ocean–atmosphere feedback term can lead to model SST drift, but it is addressed in ROMS by the linearization of an air–sea feedback parameterization term that is added to the surface heat flux. This is done using the 9-km Pathfinder climatological SSTs (Barnier et al. 1995). Because of the paucity of evaporation–precipitation forcing fields, a similar correction scheme is used for sea surface salinity (SSS).

The nested configuration requires approximately 6–8 months to reach statistical equilibrium. It is run for 10 yr in total, during which time a robust seasonal signal approximately repeats itself from at least the first year. The spinup time is estimated from surface and volume-averaged kinetic energy (KE); after the rapid adjustment of the system [~(8 months–1 yr)], statistical equilibrium is reached and the system does not exhibit any temporal drift (in energy, temperature, or salinity). The regional simulations of Marchesiello et al. (2003) and Penven et al. (2005), both using ROMS, also reveal spinup periods of less than 2 yr. Analyses for this paper are based on seasonal and monthly climatologies that are derived from the twice-daily averaged model outputs, spanning years 3–10.

The Southern African Experiment (SAfE) configuration is used as the parent domain and was designed by Penven et al. (2006a) to capture the salient oceanographic features off southern Africa. The domain is based on a Mercator grid; encompasses the region spanning 46.75°–4.8°S and 2.5°W–54.75°E; and has a horizontal resolution that ranges from 19 to 27.6 km in the north (i.e., a 230 × 194 grid), which allows for the resolution of Agulhas rings. The SAfE configuration was used by Penven et al. (2006c) to investigate the role of Madagascar in the frequency of interocean exchanges that occur south of Africa. Their work provides a validation of the SAfE configuration and shows that all of the major currents are represented realistically, in terms of both location and volume transport. In our case, the time stepping of the SAfE domain is 30 min and output is saved as twice-daily averages; 32-sigma levels define the vertical grid, which is stretched toward the surface. The boundary conditions are supplied by *WOA05* temperature and salinity climatologies, from which the geostrophic velocities are calculated, added to the Ekman transport from QuikSCAT.

The child domain has been designed to encompass the greater Benguela system, inclusive of the coastal upwelling regime as well as features of the larger-scale Benguela Current system. Embedded within the parent domain, also with 32-sigma vertical levels, it spans 35.6°–12.1°S and 3.9°–19.8°E and has a horizontal resolution that increases from 9 km in the north to 7.5 km in the south (translating into a 314 × 194 grid). The time step of the child domain is 10 min, and output is saved as twice-daily averages. The boundary conditions are supplied by the parent domain, whereas features generated at the boundaries by the child domain are allowed to feed into the parent in accordance with the two-way nesting approach.

c. Satellite data sources

Pathfinder 9-km SST climatologies are used for comparison with model-derived SSTs. The climatology has been created from daily Advanced Very High Resolution Radiometer (AVHRR) satellite data obtained between 1985 and 1999 (Armstrong and Vazquez 2001).

A second satellite SST source used is the monthly-mean climatologies of the 4.5-km Envifish product, which was derived from data obtained from January 1982 to December 1999 (Shillington and Nykjaer 2001). The higher-resolution Envifish data were degraded to better approximate the ~9-km resolution of model-derived SSTs.

The Archiving, Validation, and Interpretation of Satellite Oceanographic data (AVISO) absolute dynamic 1/3° gridded product, spanning October 1992–September 2008, was used for model–data comparisons such as surface geostrophic flows and eddy KE (EKE). The product is a sum of satellite-observed sea level anomalies and the mean dynamic topography. The latter is obtained from Rio2005 (Rio and Hernanadez 2004), which calculates the mean sea surface height (SSH) above the geoid, corrected from geophysical effects, and is based on both altimetry and in situ (i.e., hydrology and drifters) data sources. Although the AVISO gridded data products provide a rich data source from which to compare model output, it is not reliable within a 50-km coastal band.

3. Model results

Figure 2 is a twice-daily average of SSTs for 24–26 February of model year 8 and represents salient features of the Benguela upwelling system with a satisfactory degree of accuracy. The ''snapshot'' is chosen during a period of intense upwelling, particularly in the central and southern Benguela regions, so as to emphasize the upwelling front and filaments. The northern boundary of the upwelling regime is marked by the ABFZ at approximately 16°S, which is characterized by sharp alongshore temperature gradients and is consistent with the results of the satellite-based studies of Veitch et al. (2006) and Kostianoy and Lutjeharms (1999). The southern boundary is characterized by sharp offshore SST gradients and an associated equatorward jet [known as the Goodhope Jet (GHJ); Bang and Andrews 1974] as a result of the juxtaposition between the cool upwelling regime at the coast and the warm influx of water of Indian Ocean origin. The region associated with the thoroughfare of Agulhas rings and eddies has come to be known as Cape Cauldron (Boebel et al. 2003) and describes a region of turbulent interocean exchange south of 30°S that is characterized by coexisting cyclonic and anticyclonic eddies. Large filaments have been observed off the Namibian coast (Lutjeharms and Stockton 1987; Shillington et al. 1990), some of which extend up to 1300 km offshore (Lutjeharms et al. 1991). These features are intricately captured by the model that also suggests that the filaments extend farther offshore as cohesive features northward of ~28°S.

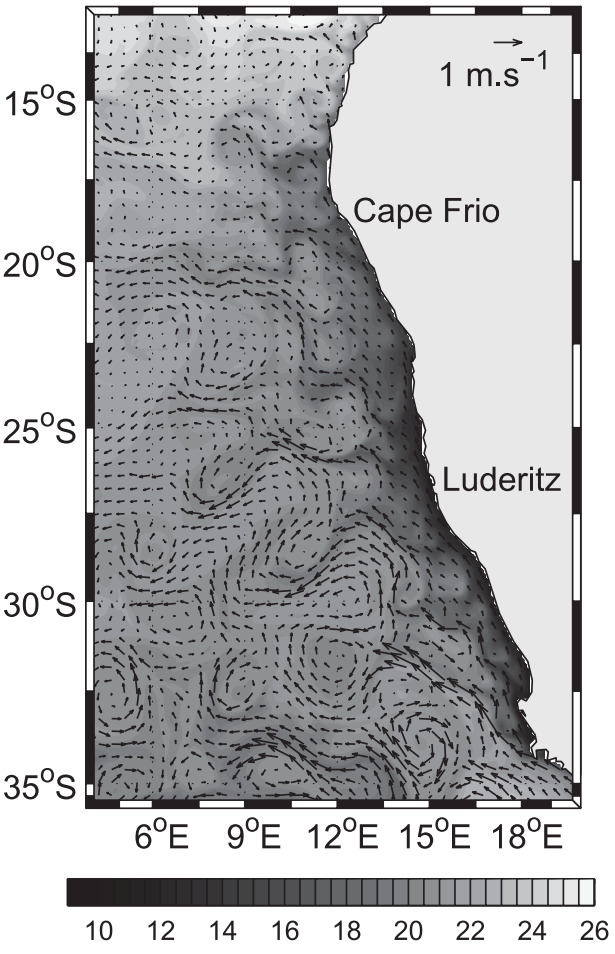

FIG. 2. Twice-daily average of model-derived SSTs (°C) for the child domain with velocity vectors (shown for every fifth grid cell) overlaid for 24–26 Feb, model year 8.

a. Comparison with data

1) SURFACE PATTERNS

Figures 3a–c show the annual (i.e., long-term mean, spanning 8 model years from model year 3 to model year 10) mean SSTs as observed by the 9-km Pathfinder satellite product, the 4.5-km Envifish product, and the equivalent as resolved by the model simulation, respectively. The model resolves a realistic pattern of annual-mean SSTs: it simulates the separation of a relatively warm offshore and characteristically cool coastal regime by a distinct upwelling front, the position of which is approximated by the location of the 17°C isotherm (shown as a white contour in Figs. 3a–c). The model also satisfactorily reproduces alongshore variations in the offshore extent of the upwelling front. Particularly, it simulates significant offshore expanses of cool water, associated with the vigorous upwelling cells at ~26°, 30°, and 32°S (i.e., the Lüderitz, Namaqua, and Columbine

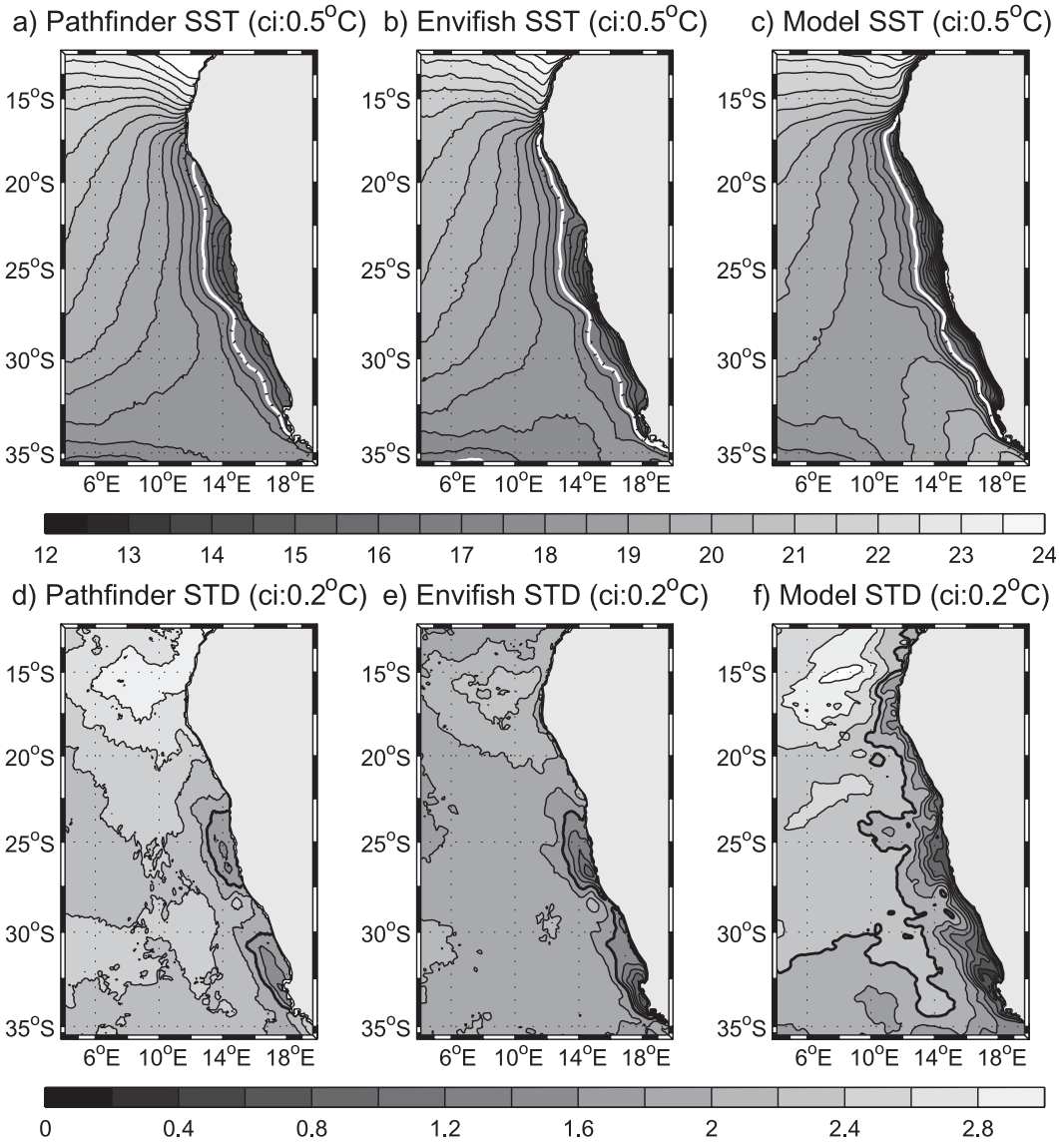

FIG. 3. (top) Annual-mean satellite [(a) Pathfinder, 9 km, and (b) Envifish, 4.5 km) and (c) model SSTs. The white contours demarcate the 17°C isotherm. The thick black dotted lines represent the approximate position of the shelf edge (~300 m). (bottom) Seasonal STDs based on satellite [(d) Pathfinder, 9 km; (e) Envifish, 4.5 km] and (f) model SSTs: the thick black lines represent 1.6°C, and the contour interval is 0.2°C.

cells, respectively). The topographical control of the upwelling front in the southern Benguela (south of ~27°S) is present in both satellite and model SSTs and is distinctly represented in Fig. 3 by the exact match of the 17°C isotherm and shelf edge (shown as a white solid line and a thick black dotted line, respectively). Satellite and model-derived SSTs show that the mean surface manifestation of the ABFZ is located at ~17°S.

Figures 3d–f show the seasonal standard deviations (STD) for Pathfinder, Envifish, and model SSTs, respectively. Although the relative patterns of seasonal SST variability are similar, differences exist in the magnitudes of variability. For both satellite products, as well as for the model-derived data, highest seasonal variability occurs in the northern part of the domain and is linked to distinct seasonal fluctuations of the intensity of the ABFZ (Veitch et al. 2006). Lowest variability occurs in the coastal regions. Although the central and southern Benguela regions have strongest seasonal upwelling signals (Lutjeharms and Meeuwis 1987; Strub et al. 1998), the SST STD is low. This is due to upwelling rates being greatest during spring and summer. The underestimation

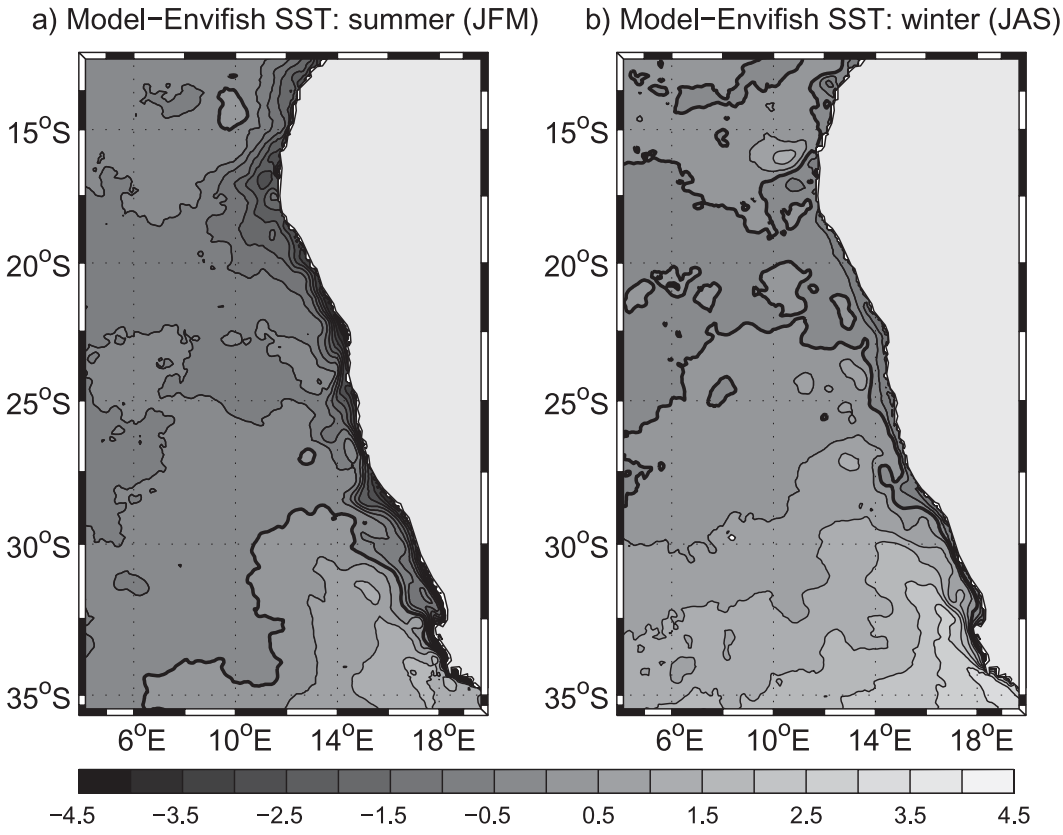

FIG. 4. Difference between satellite (Envifish) and model-derived (left) summer and (right) winter SSTs (i.e., model − satellite SST). The contour interval is 0.5°C, and the thick black line is 0°C. Positive values are regions where model SSTs are greater than satellite SSTs, negative values are regions where satellite SSTs are greater, and the bold contour represents regions of no difference.

of seasonal fluctuations in model-derived SSTs at the coast might be related to the poor coastal wind resolution, which tends to perennially overestimate coastal upwelling.

Differences between satellite and model SSTs (model − satellite) are shown in Fig. 4 for summer and winter, based on the higher-resolution Envifish dataset. Regions where satellite SSTs match model-derived SSTs are demarcated by a bold contour, positive values are where model-derived SSTs are greater, and negative values are regions where satellite SSTs are greater. A persistent difference is a warm model bias in the south, which is contained southward of ~30°S during summer and extends northward to ~25°S during winter. The source of the warm bias, particularly southward of ~30°S, is connected to an overestimation of warm Agulhas water entering the Benguela system. A similar warm bias was found by Speich et al. (2006), who ascribed it to the smoothing of model topography. The warm model bias south of ~30°S, averaged in a 100–200-km band from the shelf edge, is 0.72°C in summer and approximately doubles to 1.5°C in winter. A cool bias persists at the coast during both summer and winter months but is strongest and extends farther offshore during summer. A similar cool bias in an investigation of the Peru upwelling system using the ROMS model was noted by Penven et al. (2005) and was addressed in the earlier work of Penven et al. (2001), who ascribed it to the poor resolution of the satellite wind product at the coast (in the case of QuikSCAT is only valid beyond 50 km of the coast), such that the drop-off of the wind is not properly resolved, thereby generating too much equatorward wind stress at the coast and therefore too much upwelling (Capet et al. 2004; Colas et al. 2008a). The average cool bias on the inner shelf in the northern Benguela system (i.e., ~27°–16°S) is 2.9°C in summer and 0.65°C in winter, and the southern Benguela (i.e., ~35°–27°S) has average inner-shelf cool biases of 2.5°C in summer and 0.03°C in winter.

Figure 5 compares the surface geostrophic flow based on AVISO mean dynamic heights with that derived by model-derived SSHs and suggests that the model captures salient features of the surface geostrophic flow, which is represented by lines of constant SSH. The broad, northwestward Benguela Current and its offshore veering

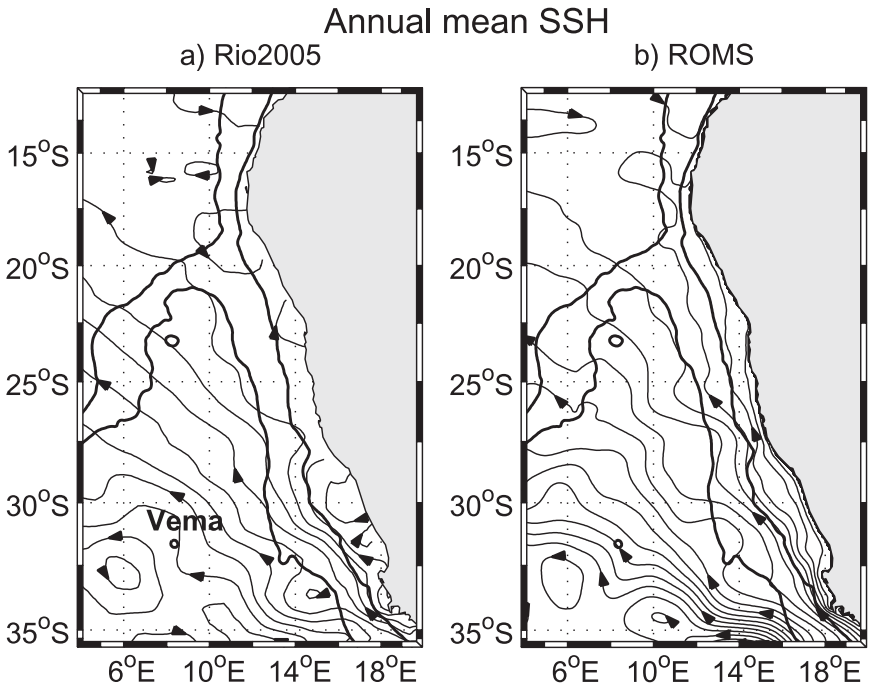

FIG. 5. Annual-mean surface geostrophic flow, indicated by the gradient of SSH, from (a) observations (Rio2005, 0.33°) and (b) model-derived data. The bold lines indicate the positions of the 300- and 3500-m isobaths. The contour interval in both is 4 cm.

from about 30°S is evident in both the model output and AVISO SSHs and is in agreement with the in situ observations of Reid (1989). South of its offshore veering, the model-derived and observed Benguela Current is characterized by two ''streams,'' separated by a conspicuous cyclonic meander. The offshore stream is situated on the western edge of the ''Agulhas eddy corridor'' (as defined by Garzoli and Gordon 1996) so that passing anticyclonic eddies enhance the mean northwestward flow in this region and inhibit it slightly offshore of the shelf edge. The meandering nature of the mean flow is therefore a manifestation of the preferential path of transient eddies in this region. Indeed, the modeling study of Matano and Beier (2003) showed that most of the energy of the Benguela Current is supplied by eddy fluxes. The inshore stream of the Benguela Current, south of its offshore veering, is subject to a strong topographical control and tends to follow alongshore variations in the shelf edge (shown as a bold contour). The topographical control is associated with the input of warmer Agulhas water and the juxtaposition of its high SSH signal with the low SSH signal of the upwelling regime on the broad shelf in the southern Benguela. This results in a significant offshore gradient of SSH and produces a geostrophically balanced current that approximately follows the alongshore run of the continental shelf. The narrowing of isolines around Cape Point is consistent with the existence of a strong equatorward jet that was anticipated and subsequently located by Bang and Andrews (1974). More specific features satisfactorily resolved by the model are an anticyclonic meander at ~27.5°S where the continental shelf narrows distinctly, and another one at the location of the Vema Seamount. South of the meandering offshore stream of the Benguela Current are two anticyclonic features of the scale of Agulhas rings located at approximately 32.5°S, 6°E and 35°S, 10°E for both model and observational sources.

No clear seasonal pattern exists in the large-scale surface geostrophic flow. Although the Benguela upwelling region has robust seasonality, the large-scale surface geostrophic flow pattern appears to be largely driven by Agulhas input in the form of filaments and eddy fluxes, which are irregular and do not have a distinct seasonal signal. This is observed in the model output on which this work is based and is in agreement with satellite observations that have been tabulated in de Ruijter et al. (1999).

Figure 6 compares time-mean satellite and model surface geostrophic EKE, which are identically calculated from AVISO and model-derived SSHs, respectively. Figures 6a,b reveal a similar pattern of lowest EKEs at the coast and over the shelf and the extremely high EKEs offshore in the southern Benguela system that we expect because of the path of Agulhas rings and eddies.

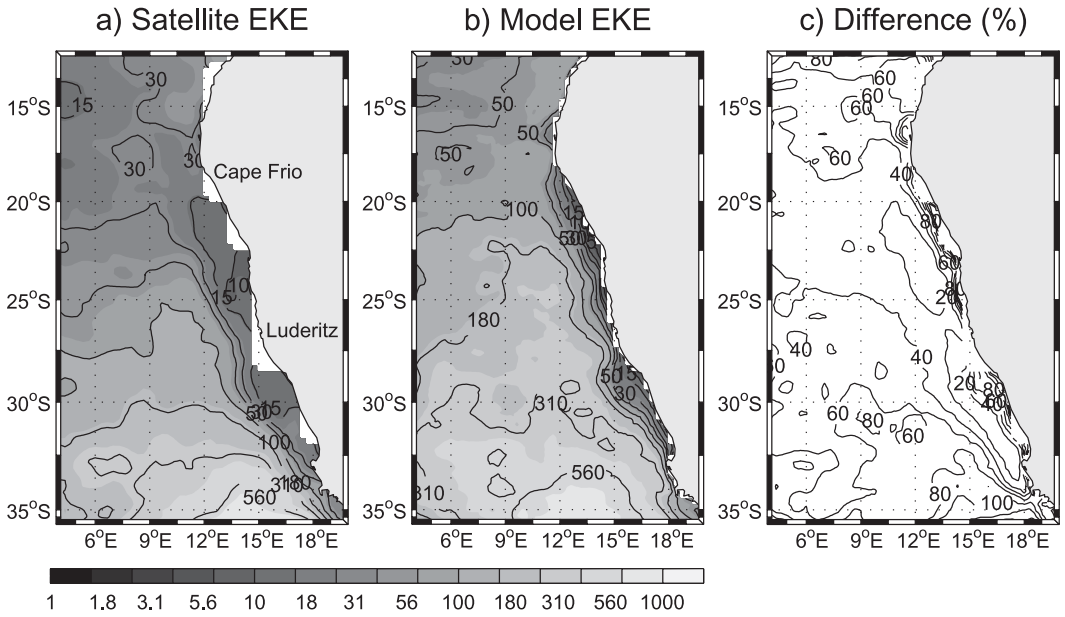

FIG. 6. (a) Satellite and (b) model-derived surface geostrophic EKE and (c) the percentage difference between the two.

Although the general pattern of model-derived surface geostrophic EKE agrees well with satellite observations, differences in magnitude exist; most generally, the model everywhere produces higher EKEs than observed by satellite. Figure 6c shows how much greater the model-derived surface EKEs are than satellite, represented as a percentage. Greatest differences occur within about 200 km of the shelf edge throughout the system to about 20°S as well as in the central offshore region. These more significant biases are related to the fact that the model overestimates the amount of Agulhas leakage into the Benguela system.

2) VERTICAL STRUCTURE

Patterns of SST (Fig. 3) suggest that a topographical control exists in the southern part of the system such that the upwelling front follows the orientation of the shelf edge. The surface geostrophic flow, as depicted in lines of constant SSH (Fig. 5), also tends to follow the undulations of the shelf edge in the southern region. The twice-daily averaged SSTs for 24–26 February of model year 8 (Fig. 2) exhibit a more realistic impression and show that from Lüderitz northward upwelling filaments tend to be more abundant and extend farther offshore than in the south. Based on these differences in surface characteristics alone, the Benguela system can be divided into distinct northern and southern regimes. To produce a representative cross section of the mean vertical structure of the northern and southern regimes, in each region a 300 km × 350 km (alongshore by cross-shore) box is placed parallel to the coast from which an alongshore average is calculated. Henceforth, all vertical sections representative of the northern and southern Benguela systems will be based on the alongshore averages of these predefined boxes, the positions of which are shown in Fig. 1.

Annual-mean temperature sections based on model-derived data are compared with the equivalent climatological mean *WOA05* sections. They are shown in Fig. 7 for the northern and southern Benguela regimes (the 16°C isotherm is highlighted in bold and approximates the location of the thermocline).

In the northern Benguela, the model simulation captures the annual-mean depth of the thermocline within 10 m of reality as depicted by *WOA05* (Fig. 7, top) data within 150 km of the coast, but the disparity increases with distance offshore. The upward slope of isotherms at the coast is present in the model output but not in the *WOA05* dataset, because it does not resolve an approximately 100-km coastal band. The downward-sloping isotherms at the shelf edge in the depth range of 100–500 m suggest a distinct poleward undercurrent (PUC) in the northern Benguela. Although downward-sloping isotherms become more distinct to at least a depth of 1000 m, the salinity structure seems to compensate for it, because the region exhibits relatively flat isopycnals (not shown) and weak currents (Fig. 13a). Though there is some indication of the downward slope of isotherms toward the coast in the *WOA05* data, particularly shallower than 200 m but also at greater depths, the coastal

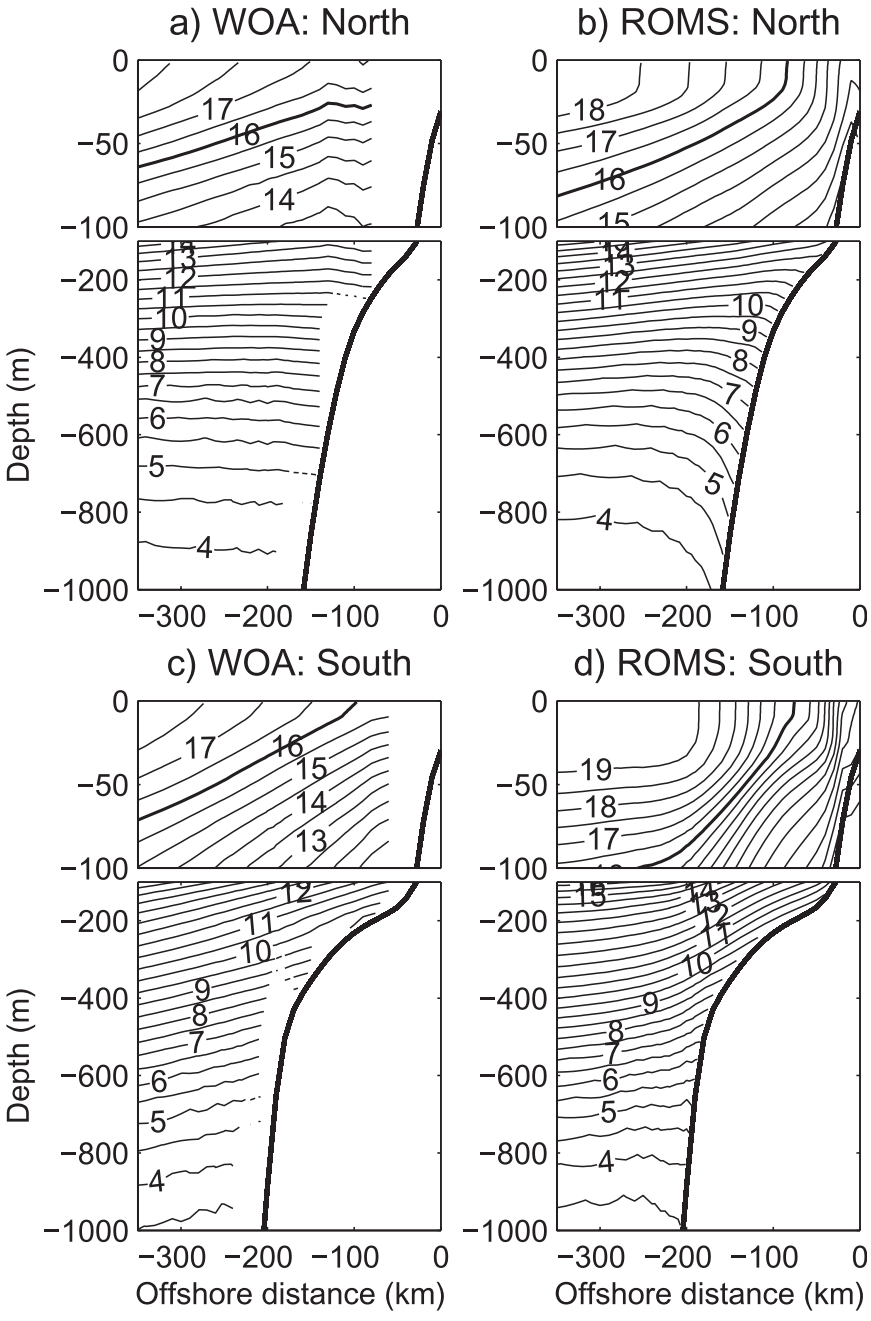

FIG. 7. Annual-mean, alongshore-averaged temperatures in regions characteristic of the (top) northern and (bottom) southern Benguela systems, from (left) *WOA05* and (right) model-derived data.

resolution is not sufficient to detect the full expanse and intensity of the poleward undercurrent.

The vertical thermal structure of the southern Benguela (Fig. 7, bottom) system differs to that of the northern Benguela in that the isotherms slope more acutely, particularly offshore of the shelf edge, in the southern Benguela. This is related to the striking juxtaposition of warm offshore water, associated with Agulhas Current input and cool water inshore, associated with the upwelling regime. The depth of the 16°C isotherm, as resolved by the model, is far deeper in the offshore regions of the southern Benguela because too much Agulhas water enters the Benguela in the model simulation. This warm bias is most pronounced in the upper

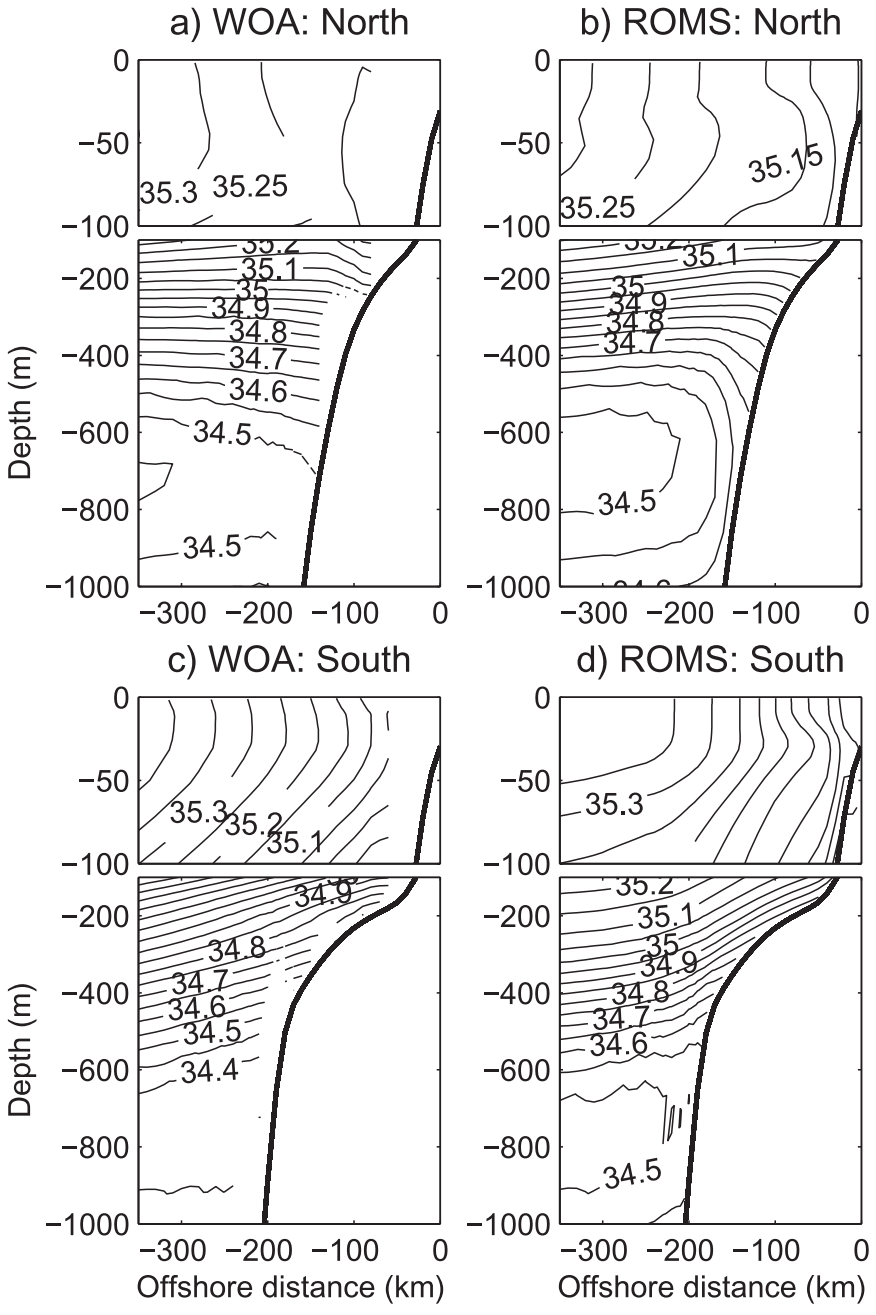

FIG. 8. As in Fig. 7, but for alongshore-averaged salinity.

150 m, whereas at greater depths the model agrees more favorably.

Distinctive of the vertical salinity structure in the northern Benguela (Fig. 8) is a high-salinity core in the vicinity of the shelf edge, for which there is evidence in both the *WOA05* and model-derived data to a depth of 200 m. More specifically, at a distance of ~100 m offshore, salinity peaks at a depth of 50 m. At depths of ~550–950 m for both *WOA05* and model-derived data is a salinity minimum layer, which is commensurate with the Antarctic Intermediate Water (AAIW) mass, whose core was located at ~750-m depth by Shannon and Hunter (1988). The salinity minimum associated with the core of the AAIW mass is 34.45 psu for *WOA05* data and 34.55 psu for the model-derived data, suggesting that the model is losing the water mass characteristics of the deep AAIW by causing it to become slightly more saline.

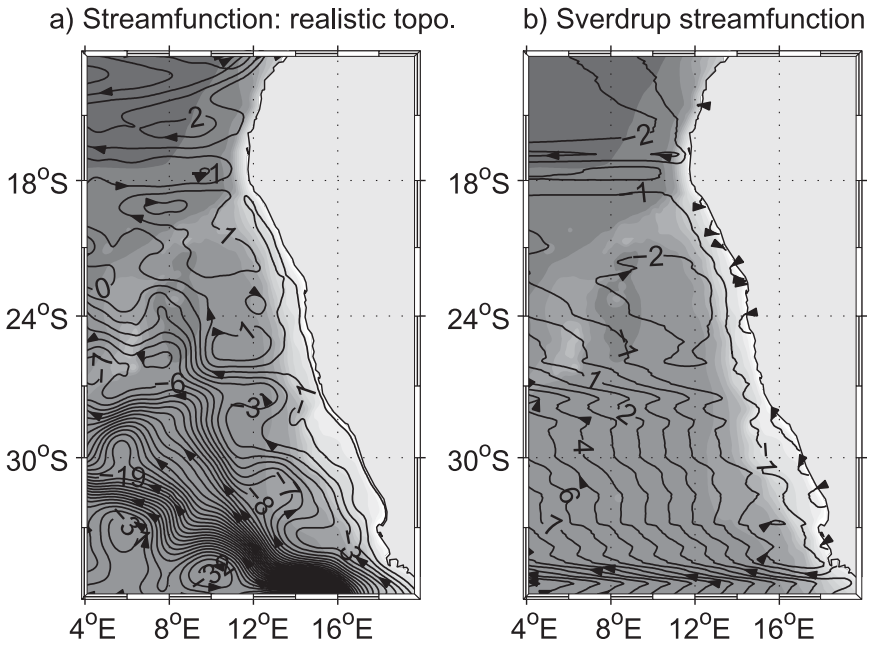

FIG. 9. (a) Annual-mean transport streamfunction, integrated from the surface to 1000-m depth, based on model output from the realistic topography simulation; (b) the Sverdrup streamfunction. Contour interval = 1 Sv. The shades of gray represent the bathymetry.

The salinity structure in the southern Benguela (Fig. 8) shows steeply sloping isolines offshore of the shelf edge and alludes to the increased storage capacity for available potential energy (APE) in this region. The model successfully reproduces a distinct halocline, but it is somewhat deeper than reality because the model overestimates Agulhas influx. The AAIW mass is again present, but it lies deeper in the southern Benguela than in the northern Benguela based on both *WOA05* and model-derived data (minimum salinity at ~800 m). The minimum salinity for this water mass is 0.1 psu less based on *WOA05* data (34.4 psu) than for model-derived data (34.5 psu), which suggests a slight loss of deep water mass characteristics.

b. Transport

1) LARGE-SCALE FLOW REGIME

Figure 9a shows the transport representative of the large-scale flow regime of the Benguela as streamlines of flow in the upper 1000 m and elucidates the division of the Benguela system into two distinct regimes, which was the focus of an investigation by Veitch et al. (2008). North of 27°S, the general flow follows the orientation of the coast and is poleward. To the south of this, the flow regime is dominated by the northwesterly meandering path of the inner and offshore branches of the Benguela Current, with the former tending to follow the orientation of the coastline until ~30°S, where it begins to veer offshore. Figure 10a shows the annual- and seasonal-mean model-derived transports across 30°S from the coast to 10°E, integrated over the upper 1000 m. Also shown (as circles) are the transport values derived from conductivity–temperature–depth (CTD) data during the second leg of the Benguela Sources and Transports survey (BEST2; 7 May–2 July 1993) for the same location (see Fig. 5 of Garzoli and Gordon 1996) from measurements taken during austral autumn. Both the observational and model-derived depth-integrated transports show that the two streams of the Benguela Current, as seen in the surface geostrophic flow regime (Fig. 5), penetrate to depths of at least 1000 m.

Figure 9b is the transport streamfunction as derived from the Sverdrup relation from the 0.5° QuikSCAT wind product and integrated from the west coast of southern Africa (i.e., the eastern boundary of the child domain). It provides convincing evidence that the poleward flow in the northern Benguela and its offshore advection at ~27°S are indeed due to the wind stress curl via the Sverdrup relation (forcing an average southward flow in the upper 1000 m at the eastern boundary on the order of ~2 cm s^{-1}). The Sverdrup relation does not hold for the southern Benguela region because of the inflow of the Agulhas Current and important eddy fluxes associated with it.

Representative of seasonal meridional transports in the southern and northern Benguela systems, Figs. 10a,b show seasonal mean transports across 30° and 23°S, respectively. During all seasons, the transport across 30°S

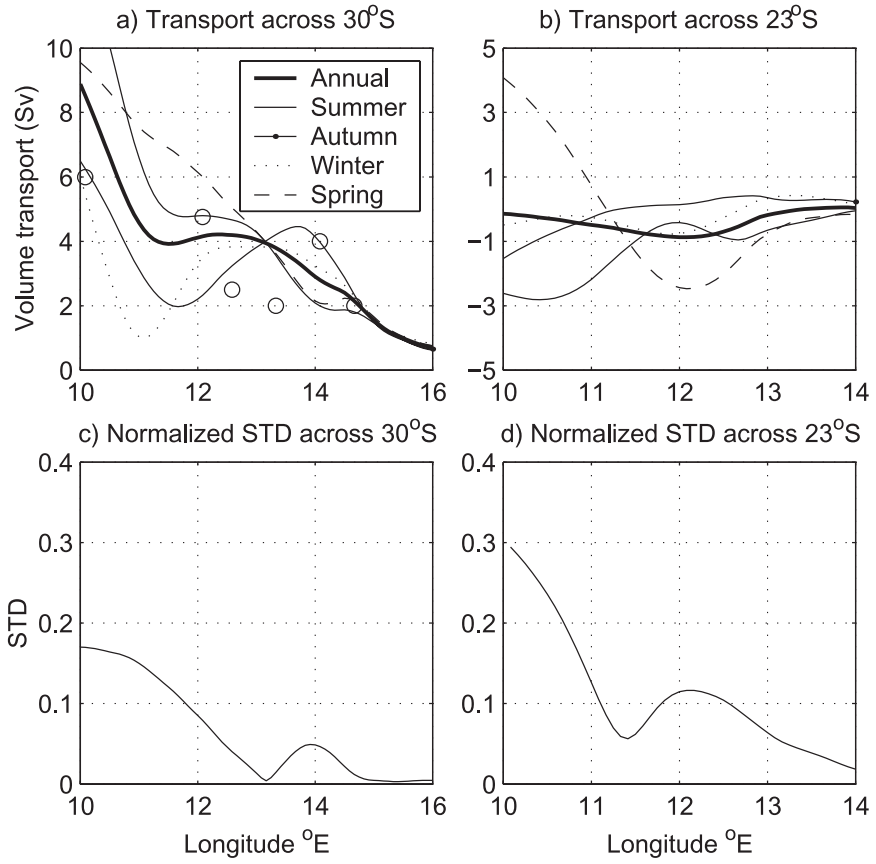

FIG. 10. Seasonal transports, integrated from the surface to 1000 m across (a) 30° and (b) 23°S. Positive is northward. Note that the scales differ for each plot. The circles in (a) are the positions of 0–1000-m transports derived from in situ data measured during austral autumn on the BEST2 (7 May–2 Jul 1993) cruise. (c),(d) The normalized seasonal STDs of (a) and (b).

is equatorward; during autumn, winter, and summer, it is characterized by a ''double peak'' separating the inshore and offshore branches of the Benguela Current. The transport across 23°S (Fig. 10b) fluctuates between poleward and equatorward with offshore distance and varies between seasons. Peak poleward transports occur across 23°S during spring and summer (farther offshore during the latter), when the cyclonic wind stress curl in this region is most intense, which is consistent with the previous finding that the poleward flow in the northern Benguela is driven by Sverdrup dynamics. Figures 10c,d are the seasonal standard deviations as a fraction of the range of transport (i.e., the normalized STDs) across 30° and 23°S, respectively. Although the poleward transport across 23°S is an order of magnitude lower than the equatorward transport across 30°S, its seasonal variability is approximately double in magnitude. The small seasonal signal of transports of the Benguela Current was also suggested by Garzoli and Gordon (1996) from their study of 16 months of in situ data.

2) SHELF-EDGE PHENOMENA

The distinctly different vertical structure of shelf-edge dynamics of the northern and southern systems and the obvious transition between them is unequivocal in Fig. 11, which shows the annual-mean alongshore, cross-shore, and vertical velocities at the shelf edge (~500 m) from 34° to 14°S. The alongshore, cross-shore, and vertical transport vectors north of ~26°S are relatively uniform, such that the poleward flow is commensurate with a predominantly downward motion. On the other hand, the meandering nature of the equatorward flow in the southern Benguela produces an alternating offshore–onshore pattern for the cross-shore component and a wave-like pattern of the alongshore velocity component associated with an alternating flow strength that results from the onshore–offshore meandering of the core of the equatorward flow.

The distinct shelf-edge poleward flow in the northern Benguela is shown in shades of gray in Fig. 11. It remains

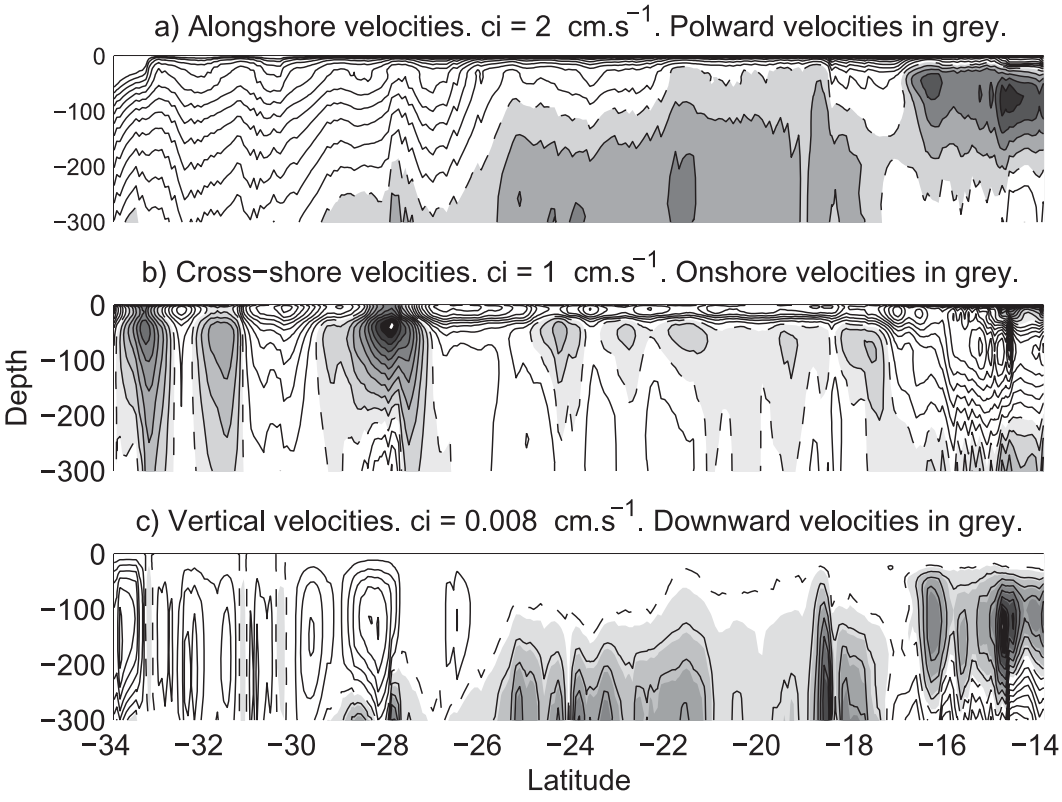

FIG. 11. Annual-mean (a) alongshore, (b) cross-shore, and (c) vertical velocities in the vicinity of the shelf edge (~500 m) from 34° to 14°S.

near surface until ~26°S, but the core starts deepening toward the south from ~22°S and this can be seen in the vertical velocity structure, in which shades of gray represent downward motion. From ~26°S southward, the poleward flow continues to deepen and no longer has a near-surface component but rather is overlaid by the meandering, equatorward flow of the coastal Benguela Current, which veers offshore significantly between ~29° and 30°S.

A simple explanation for the deepening of the poleward flow in the northern Benguela lies perhaps in the conservation of potential vorticity (PV) in a low Rossby number region where the relative vorticity term can be neglected and the potential vorticity is simplified to a relationship between planetary vorticity f and depth H of a homogeneous layer,

$$\mathrm{PV} \approx \frac{f}{H}. \tag{1}$$

A visual inspection reveals that the base of the poleward flow at 16°S is situated at approximately 300 m, thus allowing us to calculate PV. Because PV is conserved, we use Eq. (1) to calculate the changing depths H of the base of the poleward-flowing layer as it moves southward. The stars for each cross section in Fig. 12 show the depth of the poleward undercurrent as it moves southward, calculated from the potential vorticity equation. They agree relatively well with the deepening of the poleward undercurrent as resolved by the model. This suggests that the deepening of the poleward flow as it moves southward is partly a result of the conservation of potential vorticity. Penven et al. (2005) showed a similar deepening of the Peru coastal undercurrent in the Peru upwelling system.

A secondary maximum of the poleward current begins to appear at ~20°S in Fig. 12 and is particularly distinct at ~23°S, where a distinct maximum exists near the coast and the secondary maximum exists some 125 km offshore. The inshore and offshore maximums are probably the phased seasonal, upwelling-related meridional flows on the shelf and South Equatorial Undercurrent (SEUC) farther offshore, respectively, as shown in Fig. 1 of Monteiro et al. (2008). Off the Peru upwelling system, a similar double maximum of the poleward current has been simulated by Penven et al. (2005), which they suggested is commensurate with the Peru Coastal Counter Current (PCCC).

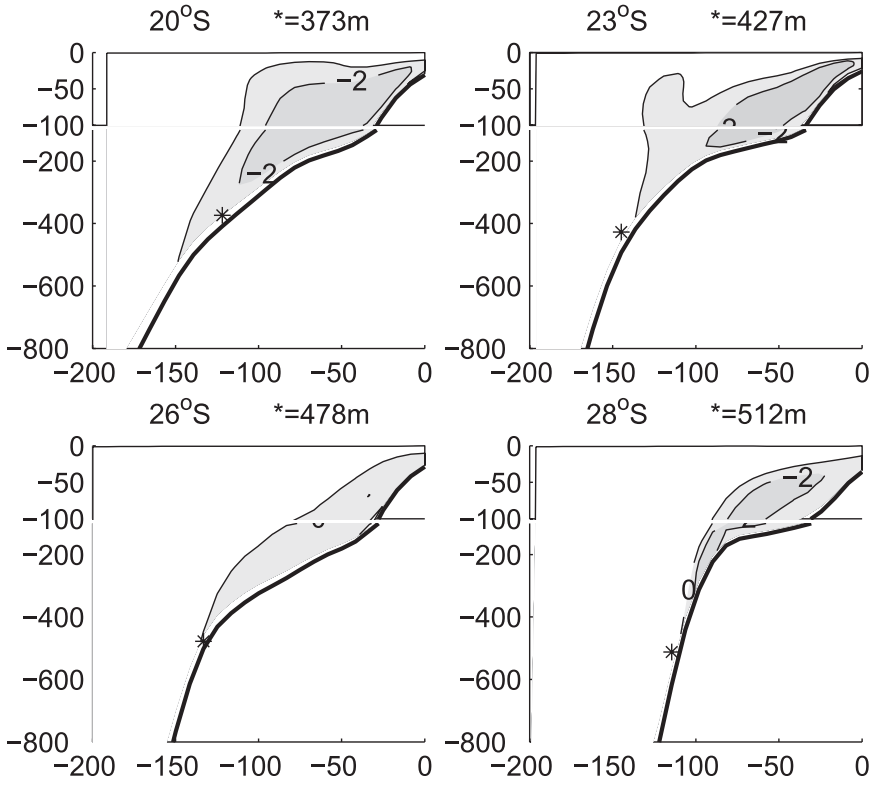

FIG. 12. Southward deepening of the poleward flow in the northern Benguela shown in several sections: 20° to 28°S. Overlaid are asterisks representing the deepening of the poleward flow based on the model of the conservation of PV in a low Rossby number regime. The *x* axis is the offshore distance in kilometers.

3) NEARSHORE FLOW STRUCTURE

The transition from large-scale, offshore circulation features to circulation patterns driven by coastal dynamics on the shelf are shown in Figs. 13 and 14 as characteristic of the northern and southern Benguela systems, respectively (based on annual-mean, alongshore averages of the three velocity components in the boxes defined in Fig. 1). The idealized upwelling circulation scenario is to some extent reflected in the annual-mean condition of both the northern and southern Benguela shelf-circulation patterns: namely, an offshore Ekman transport that is confined to the upper ~50 m and compensatory onshore and upward velocities, where the latter is within ~50 km of the coast. A distinct coastal equatorward jet with magnitudes on the order of 20 cm s^{-1} is generated in geostrophic response to upward-sloping isopycnals near the coastal boundary (e.g., see Fig. 8).

The transition from upwelling-dominated dynamics on the relatively narrow shelf to large-scale circulation features in the northern Benguela is characterized by the very distinct and shallow poleward flow situated alongside and above the shelf edge that is not part of upwelling-induced dynamics but is generated by the Sverdrup relation (see Fig. 9b). Based on a transport of 1 Sv, derived from the Sverdrup relation, across a distance of ~80 km at 24°S (see Fig. 9b), an average alongshore velocity of ~1.25 cm s^{-1} in the upper 1000 m can be inferred, which is consistent with the depth-averaged speed of the poleward flow in Fig. 13. Figure 11 shows that the poleward flow in the northern Benguela is commensurate with a downward motion that, to some extent, serves to conserve PV. To get an idea of the downward velocities that are required to conserve PV, the depth of the base of the core of the poleward flow (defined as the flow exceeding 2 cm s^{-1}) is read off Fig. 12 at 23° and 24.5°S as ~150 and ~350 m, respectively. The time it would take for a particle to travel the ~167 km between these locations at a speed of ~2 cm s^{-1} is $\sim 8 \times 10^6$ s. In this time, a particle would need to travel downward at a speed of ~0.0024 cm s^{-1} to deepen from 150 m at 23°S to 350 m at 24.5°S. Therefore, the requirement to conserve PV produces only about 16% of the total downward velocity (~0.015 cm s^{-1}, on average) associated with the path of the poleward flow, and the remainder could be accounted for by the convergence of the poleward flow at the shelf edge or by

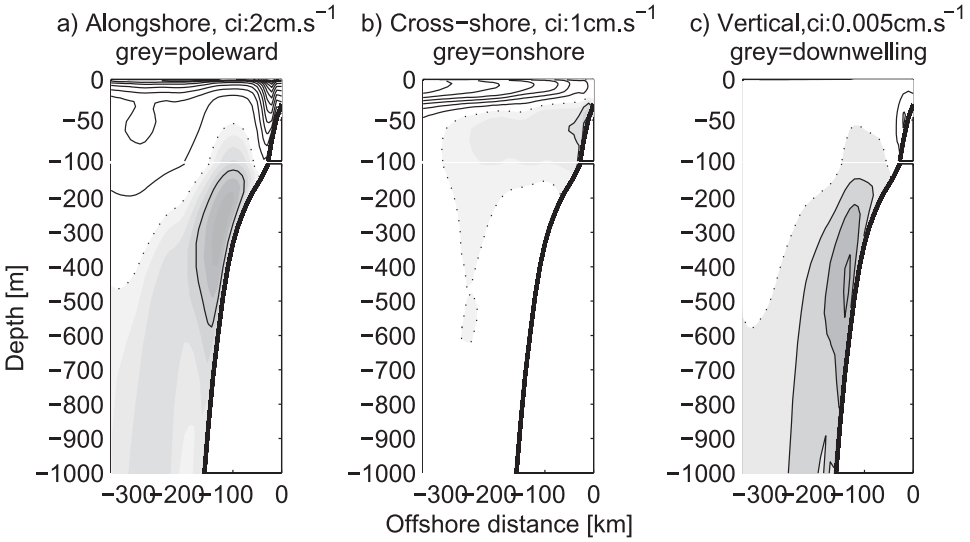

FIG. 13. Alongshore annual average of (a) alongshore, (b) cross-shore, and (c) vertical velocity components for the box defined as characteristic of the northern Benguela system in Fig. 1 (gray is poleward, onshore, and downwelling, respectively).

bottom Ekman dynamics. To get an estimate of the downward velocity that would result from the bottom Ekman layer, we assume constant vertical mixing and neglect the effect of the slope (on the Ekman layer). Based on Eq. (41) in Kundu (1990, p. 494), a bottom velocity of 2.5 cm s^{-1}, and an Ekman depth of 30 m, we approximate a maximum downward Ekman velocity of 0.006 cm s^{-1}. Although this method is rather vague, it does suggest that a dominant factor in the downward velocities at the shelf in the northern Benguela is bottom Ekman friction. The only distinct seasonal fluctuation of nearshore dynamics of the northern Benguela shelf is associated with the poleward flow, which is in excess of 4 cm s^{-1} during spring and summer and is 2–2.5 cm s^{-1} during autumn and winter.

The broad shelf in the southern Benguela is characterized by upwelling dynamics on the inner-shelf region and relative quiescence on the midshelf region. Large-scale circulation features in the southern Benguela significantly influence shelf-edge dynamics but in the mean state do not impinge on the wide midshelf region. Figure 14 reveals the important phenomenon of the splitting of the equatorward jet as it passes Cape Columbine (CC), such that one branch approximately follows the shelf edge and

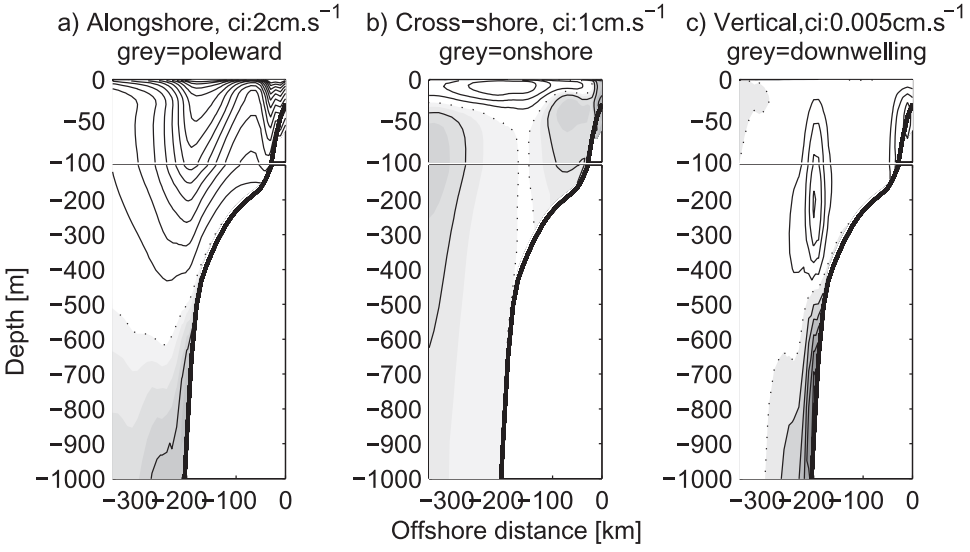

FIG. 14. As in Fig. 13, but for the box defined as characteristic of the southern Benguela system in Fig. 1.

the other veers offshore as observed by Shannon (1985), Boyd et al. (1992), and Stenevik et al. (2008) and is simulated by the model. The importance of this feature is in the transportation of fish eggs and larvae into the St. Helena Bay nursery area (e.g., Penven 2000; Stenevik et al. 2008). Shelf-edge upwelling in the southern Benguela can be seen in Fig. 14c and is a result of the flow divergence caused by the splitting of this equatorward jet. The shelf-edge upwelling feature exists year-round, as does the splitting of the shelf-edge equatorward jet. Although Barange and Pillar (1992) observed a secondary, topographically forced shelf-edge upwelling feature in the northern Benguela at 20° and 26°S and Nelson and Hutchings (1983) suggested that shelf-edge upwelling features are prone to exist northward of Cape Columbine at 32°S, our model results suggest that shelf-edge upwelling is a robust feature in the southern Benguela, rather than in the north.

4) COASTAL UPWELLING

The ecological and economic importance of the Benguela upwelling system has encouraged consistent research since at least the 1960s. The model output on which this work is based, inclusive of the whole Benguela upwelling system, provides the means to clarify sparse in situ and satellite-based estimations of upwelling locations, intensities, and seasonal signals. We compute the annual-mean upwelling fluxes, based on Ekman transport velocities [derived from the alongshore wind stress and known as the Bakun upwelling index (BUI)] and model-derived vertical velocities (MUI). Our calculation of alongshore wind-derived upwelling velocities is based on the Ekman coastal upwelling index (CUI) derived by Bakun (1973), which appears as follows:

$$E_k = \frac{\tau_{\text{alongshore}}}{L_u \rho_0 f}, \tag{2}$$

where E_k is the upwelling velocity in m s^{-1}, $\tau_{\text{alongshore}}$ is the alongshore wind stress component in N m^{-2}; and L_u is the width of active Ekman divergence and is frequently and mistakenly taken to be commensurate with the internal Rossby radius, which describes the cross-shore scale of geostrophic adjustment scale of the pycnocline slope and not the upwelling cell structure (see Estrade et al. 2008). For L_u, we use the formulation of Estrade et al. (2008), who developed an analytical model of two-dimensional upwelling to show that the cross-shore width of active upwelling can be better approximated as

$$L_u = \frac{0.75D}{S}, \tag{3}$$

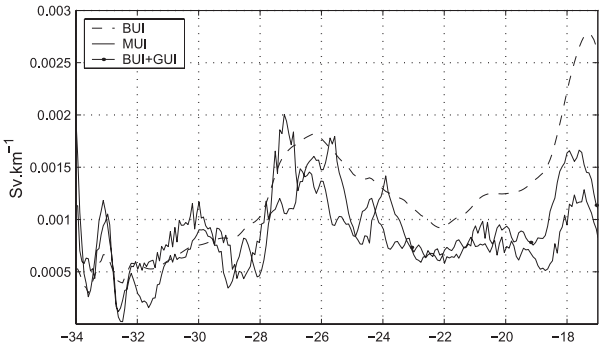

FIG. 15. Annual-mean upwelling fluxes, based on the BUI (dashed line), model-derived vertical velocities (solid line), and BUI + GUI (dotted–dashed line).

where D is the depth of the Ekman layer and S is the slope of the shelf. We calculate the average slope over the shelf for each cross-shelf section and define the Ekman layer depth as 30 m based on Fig. 8, which is consistent with in situ data for Cape Columbine (Johnson and Nelson 1999). Based on slopes calculated from model bathymetries and the previously stated Ekman layer depth, we obtain L_u values ranging from <10 km north of 20°S where the shelf is shallow to >30 km in the south where the shelf is broad. Between ~20° and 30°S, the value of L_u is more or less constant and is approximately 12 km. The Ekman transport velocities are then integrated in the alongshore and cross-shore directions [within the zone of Ekman divergence, calculated in Eq. (3)] to obtain annual-mean upwelling fluxes (BUI) that are shown in Fig. 15 in units of Sv km^{-1}. Our results are on the order of the estimates of Carr and Kearns (2002), who used the *European Remote Sensing Satellite-2* (*ERS-2*) wind product to calculate their fluxes (their units are shown in m^2 s^{-1}, or m^3 s^{-1} m^{-1}). However, their results are somewhat lower than ours and could be due to differences in the definition of L_u. For instance, at the Namibia upwelling cell (at ~21°S), their annual-mean estimate is ~0.0005 Sv km^{-1}, whereas our estimate is ~0.000 75 Sv km^{-1}.

Results of the more direct method of calculating upwelling fluxes by extracting model-derived upwelling velocities at the base of the Ekman layer and integrating alongshore and cross-shore (within the width of L_u) is shown as a solid line in Fig. 15. Model-derived upwelling fluxes suggest that upwelling intensity along the coast is far from contiguous but instead is characterized by a number of cells of enhanced activity, which on the smaller scale is related to the orientation of the coastline (Shannon and Nelson 1996). A similar pattern is present in Ekman transport fluxes shown as a dashed line in Fig. 15; however, the prominent peaks of the cells are

underestimated. A significant disparity between model-generated upwelling fluxes and those derived from the Ekman transport formulation is that, north of approximately 25°S, the latter consistently exceeds the former. This is a result of geostrophic convergence, which will be investigated further in the next section.

The out of phase seasonal pulsing of the upwelling cells to the north and south of Lüderitz was discussed by Veitch et al. (2008), who were able to clarify and improve upon historical results based on sparse in situ data as well as results obtained from relatively coarse-resolution satellite products. Their results revealed the perennial nature of the Lüderitz upwelling cell (situated at ~27.5°S) flanked by the strongly seasonal cells to the south [Cape Peninsula (CP) at ~34°S, Cape Columbine at ~33°S, and Namaqua at ~30°S] with peak upwelling rates in spring and summer and the weakly seasonal cells to the north (Walvis Bay at ~24°S, Namibia at ~21°S, and Cunene at ~18°S) with slight maximum upwelling signals in winter.

5) GEOSTROPHIC CONVERGENCE

The role of geostrophic convergence in modulating upwelling fluxes has been investigated off the coast of Peru during both the 1982/83 and the 1997/98 El Niño events. The former was studied by Huyer et al. (1987) using observational data, whereas the latter was investigated by Colas et al. (2008b) using a numerical model. Geostrophic convergence has also recently been investigated off the coast of New Caledonia by Marchesiello and Estrade (2010). They formulated an index for coastal upwelling in which they introduced a geostrophic upwelling index (GUI) term into the traditional Bakun index [Eq. (2)], so that their CUI appears as follows:

$$\mathrm{CUI} = \frac{\tau_{\mathrm{alongshore}}}{L_u \rho f} + \mathrm{GUI}, \tag{4}$$

where GUI is upwelling related to geostrophic currents alone and appears as follows:

$$\mathrm{GUI} = -\int_{x=0}^{x=L_u} \int_{z_0}^{0} \left(\frac{\partial u_g}{\partial x} + \frac{\partial v_g}{\partial y} \right) \partial z \, \partial x, \tag{5}$$

where z_0 is the depth of the Ekman layer and u_g and v_g are the cross-shore and alongshore geostrophic velocity components (calculated using the thermal wind relation, with the model-derived density field and then rotated to align parallel and perpendicular to the coast). A second formulation of GUI was derived for narrow shelf regions that approximated wall boundary conditions (where the onshore velocity component is directly converted into vertical velocities by the discreet continuity equation at the wall):

$$\mathrm{GUI} = -\frac{1}{L_u} \int_{z_0}^{0} u_g \, \partial z. \tag{6}$$

In Fig. 15, along with annual-mean Bakun upwelling index (dashed line) and the modeled upwelling fluxes (solid line), we show the BUI corrected with the GUI derived by Marchesiello and Estrade (2010; dotted–dashed line) to take into account the inhibition or enhancement of coastal upwelling by geostrophic currents. The correction of the Bakun upwelling index for geostrophic convergence reveals a much better agreement with the modeled upwelling fluxes, as can be seen in Fig. 15. The fact that modeled upwelling fluxes are less than those predicted by the Bakun upwelling index is a result of the inhibition of upwelling by geostrophic currents that converge at the coast and lead to downwelling. Marchesiello and Estrade (2010) similarly noted an overestimation of upwelling fluxes by the Bakun index in the northern Benguela and related it to eastward equatorial currents that feed into the cyclonic Angola Dome. Their work highlighted parallels between the tropical regions of the Canary and Peru upwelling systems by suggesting the role of the Guinea and Peru Domes in counteracting coastal upwelling by geostrophic convergence. In the far south (specifically at ~33°S), the Bakun upwelling index underestimates the upwelling rate, suggesting that there is geostrophic divergence in this area resulting in enhanced upwelling rates. The correction of the Bakun index for geostrophic convergence (or, in this case, divergence) for the southern part of the system shown in the dotted–dashed line in Fig. 15 shows that upwelling is indeed enhanced by geostrophic upwelling (i.e., the addition of the GUI to the BUI results in an upwelling index more comparable to modeled vertical velocities).

c. *Topographical control*

The extent to which topographical features influence the large-scale circulation and coastal upwelling regime is investigated by rerunning the Benguela reference simulation, but with a smoothed coastline and topography (between 32° and 21°S; refer to Fig. 16). The topography remains unchanged over and north of the Walvis Ridge to retain its influences on circulation features and not to complicate the effect of removing alongshore variations in the shelf and coastline.

Figure 17a shows the 0–1000-m integrated transport streamfunction for the smoothed topography simulation;

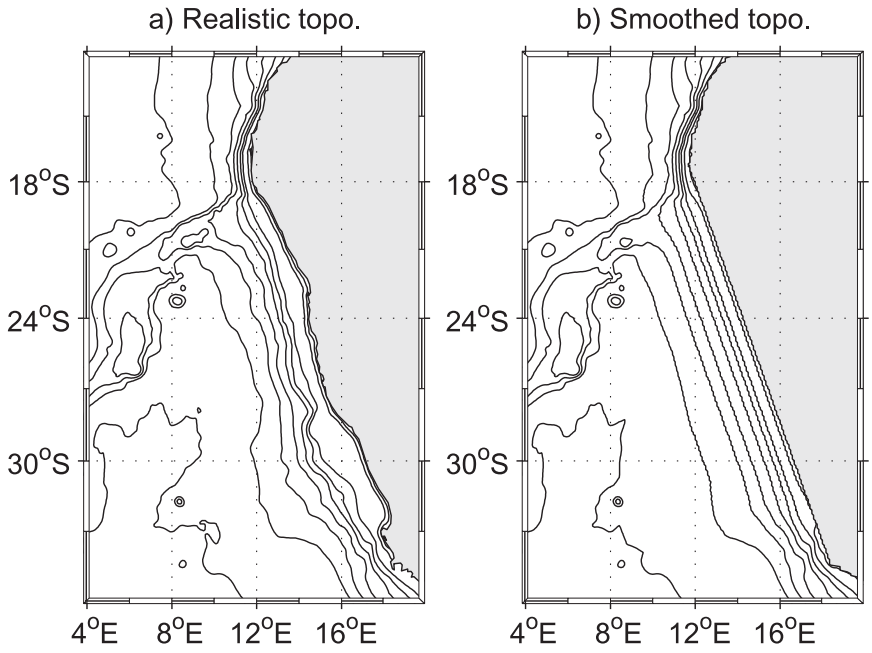

FIG. 16. Topography of (a) reference and (b) smoothed shelf and coastline experiment.

compared with the transport streamfunction for the reference experiment (Fig. 9a), it suggests that the distinct nature of the separation of the large-scale flow regimes of the northern and southern Benguela systems is to some extent topographically driven. Evidence of this lies in the fact that the very distinct offshore transport that is coincident with the discontinuity of the shelf edge in Fig. 9a is not prominent in the smoothed topography experiment (Fig. 17a). The anticyclonic meander at the transition region, in the vicinity of the Lüderitz upwelling cell (~29°–27°S), is not present in the straight coastline simulation, suggesting that the sudden narrowing of the shelf at this location has important implications for the cross-shelf exchange of water mass properties and therefore also for the productivity of the coastal upwelling region. The equatorward regime of the southern Benguela system (previously defined as south of ~28°S) extends farther north in the region ~300 km from the coast. The meandering nature of the equatorward flow of the reference simulation, particularly in the offshore region, is likely related to the mean-state manifestation of mesoscale features; nearer to the shelf edge, it also seems to be topographically controlled. Therefore, in the case of the smoothed coastline experiment, the equatorward flow over the straightened shelf does not meander as much as in the reference simulation. This is manifested as a stronger equatorward transport for the smoothed coastline experiment across 30°S within ~300 km of the coast (refer to Fig. 17b). The poleward flow in the northern Benguela that has been related to the Sverdrup relation persists in the smoothed coastline experiment but is confined to a narrower band because of differences in its interaction with the more intense equatorward flow (Fig. 17c).

Upwelling fluxes, based on model-derived vertical velocities for the smoothed topography simulation, are shown in Fig. 18a along with the fluxes derived in the reference experiment (dashed and solid lines, respectively). The smoothed topography coastline experiment results in an upwelling zone that is more or less contiguous in the alongshore direction, with a slight peak in the vicinity of Lüderitz resulting from the stronger alongshore wind stress and wind stress curl; however, in general, the fluxes are lower than the peak fluxes resolved by the reference experiment. This suggests that alongshore topographical variations have an important role to play in enhancing upwelling fluxes. Indeed, numerical (Peffley and O'Brien 1976; Gan and Allen 2002a) and laboratory (Narimousa and Maxworthy 1986) studies have demonstrated the enhancement of upwelling downstream of topographical capes. Figure 18b shows the orientation of the Benguela coastline in degrees (toward the west) from north of the Benguela system. The solid vertical arrows highlight the connection of peak upwelling regions with locations where the coastline veers toward the east (sudden changes in the orientation of the coastline represents the locations of prominent capes) and indeed implies an enhancement of upwelling intensity downstream (northern edge) of capes.

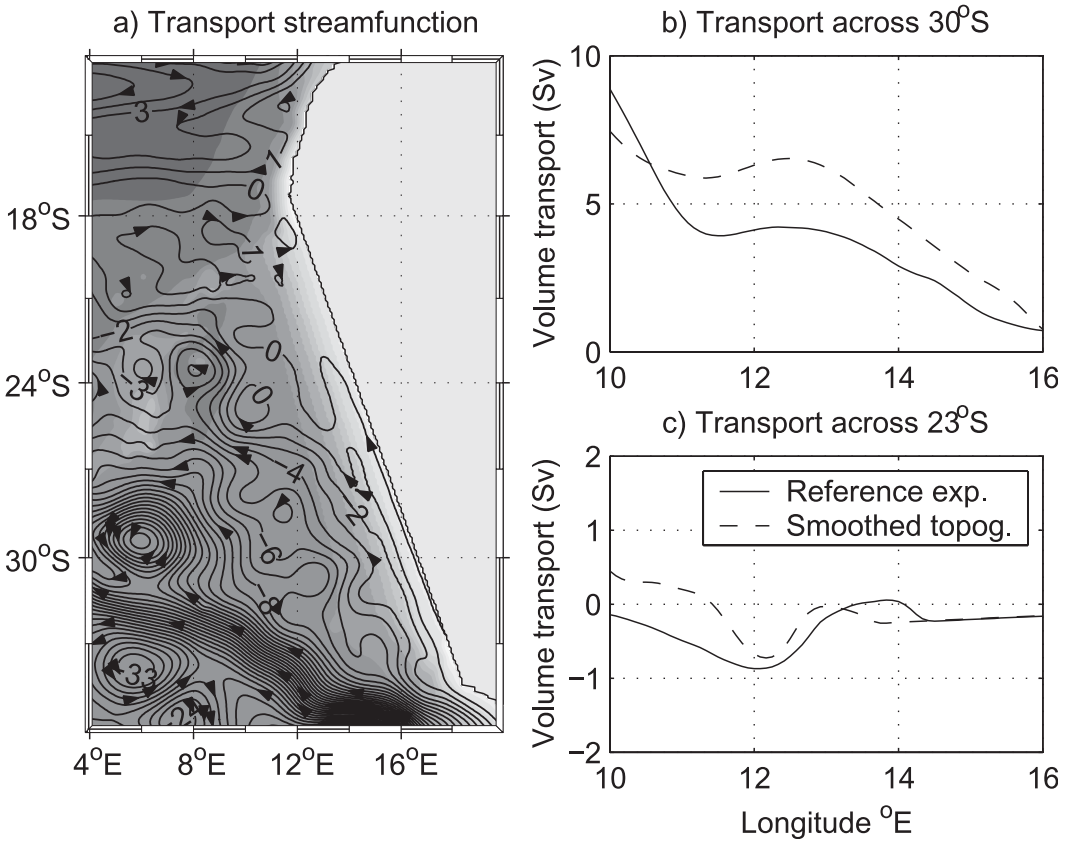

FIG. 17. (a) Transport streamfunction (0–1000 m) and alongshore transport across (b) 30°S and (c) 23°S for the reference (solid line) and smoothed topography (dashed line) simulations.

4. Discussion

Equilibrium dynamics of the greater Benguela system has been addressed with the use of a ROMS climatologically forced numerical model. Although research of the Benguela upwelling system goes far back, our model simulation has provided the first opportunity to study salient features of the system in a spatially and temporally cohesive manner. Our simulation has allowed us to unequivocally explain the nature, origin, and seasonal cycle of features that until now have been poorly understood because of the sporadic nature of observational data in this region. Some of the key features that we have provided a better understanding on, based on our simulation, are described in this section.

Variability and fluxes across the dynamic northern and southern boundaries can have significant ecological implications for the Benguela upwelling system. For example, Monteiro and van der Plas (2006) show that coastal hypoxia in the central Benguela is predominantly driven by advected oxygen fluxes from source waters in the Angola Dome region north of the ABFZ and intensifies during late austral summer when the shelf poleward flow strengthens. The ROMS simulation resolves this poleward flow, as well as its seasonal cycle, and provides insight into its fate as it travels southward. The wind stress curl (via the Sverdrup relation) has been shown to be the driving force of the poleward flow, which is strongest during spring and summer, when the wind stress curl is most negative. As it flows southward, it deepens and between ~25° and 27°S much of it veers offshore. The offshore veering is related to the nature of the wind stress curl interacting with the northwestward path of the Benguela Current and is further influenced by alongshore topographical variations. Boundary conditions of the Benguela upwelling system, south of ~30°S, are commensurate with the path of Agulhas rings and eddies that, in the mean state, are represented by the meandering nature of the Benguela Current. Farther inshore, the time-mean Benguela Current tends to be topographically controlled as it follows the run of the shelf edge. The inshore, topographically controlled, and meandering offshore streams of the Benguela Current do not exhibit a distinct seasonal signal.

The model distinctly resolves all seven of the major upwelling cells that have been observed in its domain:

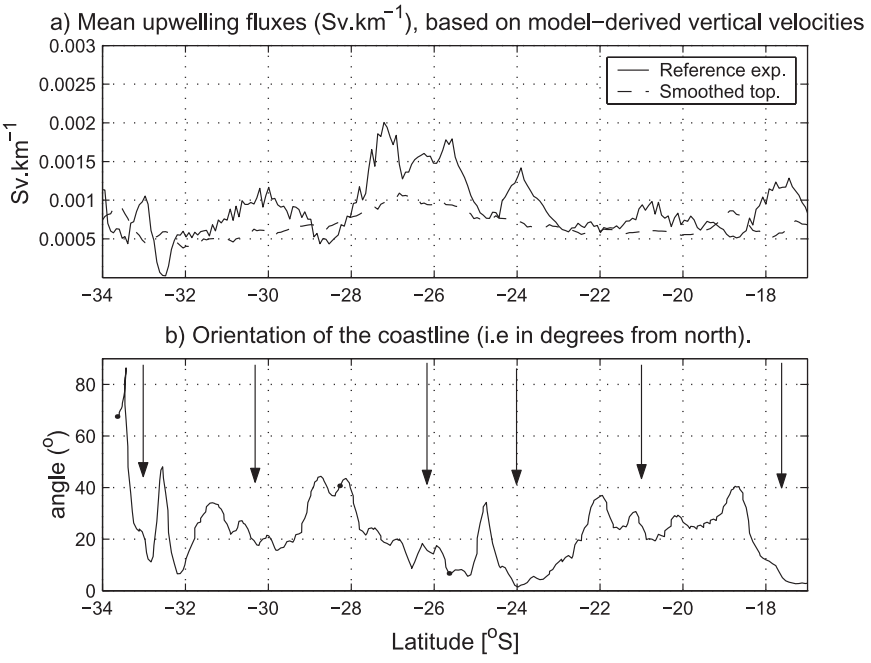

FIG. 18. (a) Annual-mean upwelling fluxes for the reference (solid line) and smoothed topography (dashed line) simulations. The gray line is the Ekman transport flux for the smoothed topography simulation. (b) Orientation of the coastline (degrees from north).

namely (from the south), Cape Peninsula, Cape Columbine, Namaqua, Lüderitz, Walvis Bay, Namibia, and Cunene (or Cape Frio). The three southernmost cells have the most seasonal variability, experiencing the greatest upwelling during spring and summer months and the least upwelling during autumn and winter. Based on model-derived vertical velocities, average upwelling rates in the southern Benguela during periods of most active upwelling is on the order of 7 m day^{-1}. By calculating the apparent uplift of isanosteres (lines of constant thermosteric anomaly) obtained from two cruises during active upwelling in the southern Benguela, Andrews and Hutchings (1980) estimated an average apparent uplift of 21 m day^{-1}. Their estimate is significantly higher than the model-derived upwelling rates, but their method is subject to an inherent inaccuracy based on the fact that some of the uplift must be related to mixing processes. Furthermore, the model-derived peak upwelling season is subject to a climatological forcing, which underestimates highest and lowest alongshore wind stresses. Peak upwelling in the Benguela occurs throughout the year at the Lüderitz upwelling cell, where there is very little seasonal variability. The annual-mean upwelling rate in this region is ~13 m day^{-1}, which transpires into an average flux of 1.8 Sv. Our investigation has shown that the Bakun upwelling index significantly overestimates upwelling fluxes in the northern Benguela system. We included the effect of geostrophic convergence to the traditional Bakun upwelling index and were consequently able to show that coastal upwelling in the northern Benguela is inhibited by converging geostrophic currents at the coast. The topographical effect on upwelling in the Benguela has been investigated by smoothing the shelf and coastline in the alongshore direction. This has allowed us to show that alongshore variations in the coastline and topography have the effect of enhancing upwelling on the downstream side of capes. This is in line with experimental numerical simulations that have unequivocally revealed the role of topography in locally enhancing upwelling in the vicinity of capes.

An example of the successful application of this ROMS simulation is its coupling with an individual-based model to better understand the transport of ichthyoplankton across the Lüderitz Upwelling Cell–Orange River Cone (LUCORC) barrier (Lett et al. 2007). The quality of the hydrodynamic output of the model has now been thoroughly tested and will be useful in driving biological modeling studies in the various regions thought to be critical to ecosystem functioning.

Acknowledgments. The authors are grateful for BCLME funding that provided servers within the Department of Oceanography, UCT, on which our simulations were initially run. The use of the high performance computing facility (CAPARMOR) at IFREMER, Brest, is also greatly appreciated, as is the availability of the

Center for High Performance Computing (CHPC) in Rosebank, Cape Town. JAV gratefully acknowledges funding from the National Research Foundation in South Africa and a DSF bursary from the IRD.

REFERENCES

Andrews, W. R. H., and L. Hutchings, 1980: Upwelling in the southern Benguela Current. *Prog. Oceanogr.,* **9,** 1–8.

Armstrong, E., and J. Vazquez, 2001: A new global satellite-based sea surface temperature climatology. *Geophys. Res. Lett.,* **28,** 4199–4202.

Bakun, A., 1973: Coastal upwelling indices, west coast of North America, 1946-71. NOAA Tech. Rep. NMFS SSRF-671, 103 pp.

Bang, N., and W. Andrews, 1974: Direct current measurements of a shelf-edge frontal jet in the southern Benguela system. *J. Mar. Res.,* **32,** 405–417.

Barange, M., and S. Pillar, 1992: Euphausiacea in the northern Benguela upwelling system. *Cont. Shelf Res.,* **12,** 1027–1042.

Barnier, B., L. Siefridt, and P. Marchesiello, 1995: Thermal forcing for a global ocean circulation model using a three-year climatology of ECMWF analysis. *J. Mar. Syst.,* **6,** 363–380.

Blanke, B., S. Speich, A. Bentamy, C. Roy, and B. Sow, 2005: Modeling the structure and variability of the southern Benguela upwelling using QuikSCAT wind forcing. *J. Geophys. Res.,* **110,** C07018, doi:10.1029/2004JC002529.

Boebel, O., J. Lutjeharms, C. Schmid, W. Zenk, T. Rossby, and C. Barron, 2003: The Cape Cauldron: A regime of turbulent inter-ocean exchange. *Deep-Sea Res. II,* **50,** 57–86.

Boyd, A. J., J. Taunton-Clark, and G. Oberholzer, 1992: Spatial features of the near-surface and midwater circulation patterns off western and southern South Africa and their role in the life histories of various commercially fished species. *S. Afr. J. Mar. Sci.,* **12,** 189–206.

Capet, X. J., P. Marchesiello, and J. C. McWilliams, 2004: Upwelling response to coastal wind profiles. *Geophys. Res. Lett.,* **31,** L13311, doi:10.1029/2004GL020123.

Carr, M.-E., and E. Kearns, 2002: Estimation of potential productivity in eastern boundary currents using remote sensing. *Deep-Sea Res. II,* **49,** 59–80.

Colas, F., X. Capet, X. Jin, J. Molemaker, D. Chelton, and J. McWilliams, 2008a: Wind stress and sea surface temperature coupling in eastern boundary upwelling systems. *Proc. Eastern Boundary Upwelling Ecosystems Symp.,* Las Palmas, Canary Islands, 107.

——, ——, J. C. McWilliams, and A. Shchepetkin, 2008b: 1997–1998 El Niño off Peru: A numerical study. *Prog. Oceanogr.,* **79,** 138–155.

Colberg, F., and C. J. C. Reason, 2006: A model study of the Angola Benguela Frontal Zone: Sensitivity to atmospheric forcing. *Geophys. Res. Lett.,* **33,** L19608, doi:10.1029/2006GL027463.

Conkright, M., R. Locarnini, H. Garcia, T. O'Brien, T. Boyer, C. Stephens, and J. Antonov, 2002: World Ocean Atlas 2001: Objective analyses, data statistics and figures. National Oceanographic Data Center Internal Rep. 17, 21 pp.

Da Silva, A., C. Young, and S. Levitus, 1994: Atlas of surface marine data 1994. Vol. 1: Algorithms and procedures. NOAA Tech Rep., 117 pp.

Debreu, L., and E. Blayo, 2008: Two-way embedding algorithms: A review. *Ocean Dyn.,* **58,** 415–428.

de Ruijter, W., A. Biastoch, S. Drijfhout, J. Lutjeharms, R. Matano, T. Pichevin, P. van Leeuwen, and W. Weijer, 1999: Indian-Atlantic interocean exchange: Dynamics, estimation and impact. *J. Geophys. Res.,* **104** (C9), 20 885–20 910.

Estrade, P., P. Marchesiello, A. Colin de Verdiere, and C. Roy, 2008: Cross-shelf structure of coastal upwelling: A two-dimensional expansion of Ekman's theory and a mechanism for innershelf upwelling shut down. *J. Mar. Res.,* **66,** 589–616.

Gan, J., and J. S. Allen, 2002a: A modeling study of shelf circulation off northern California in the region of the Coastal Ocean Dynamics Experiment: Response to relaxation of upwelling winds. *J. Geophys. Res.,* **107,** 3123, doi:10.1029/2000JC000768.

Garzoli, S., and A. Gordon, 1996: Origins and variability of the Benguela Current. *J. Geophys. Res.,* **101** (C1), 897–906.

Gordon, A., 2003: The brawniest retroflection. *Nature,* **421,** 904–905.

——, J. Lutjeharms, and M. Grundlingh, 1987: Stratification and circulation at the Agulhas Retroflection. *Deep-Sea Res.,* **34,** 565–599.

——, R. Weiss, W. Smethie, and M. Warner, 1992: Thermocline and intermediate water communication between the South Atlantic and Indian Oceans. *J. Geophys. Res.,* **97** (C5), 7223–7240.

Huyer, A., R. Smith, and T. Paluszkiewicz, 1987: Coastal upwelling off Peru during normal and El Niño times, 1981–1984. *J. Geophys. Res.,* **92,** 14 297–14 307.

John, H.-C., V. Mohrholz, and J. Lutjeharms, 2001: Cross-front hydrography and fish larval distribution at the Angola-Benguela Front. *J. Mar. Syst.,* **28,** 91–111.

Johnson, A., and G. Nelson, 1999: Ekman estimates of upwelling at Cape Columbine based on measurements of longshore wind from a 35-year time-series. *S. Afr. J. Mar. Sci.,* **21,** 433–436.

Kostianoy, A., and J. Lutjeharms, 1999: Atmospheric effects in the Angola-Benguela frontal zone. *J. Geophys. Res.,* **104,** 20 963–20 970.

Kundu, P. K., 1990: *Fluid Mechanics*. Academic Press, 639 pp.

Large, W., J. McWilliams, and S. Doney, 1994: Oceanic vertical mixing: A review and a model with a nonlocal boundary layer parameterization. *Rev. Geophys.,* **32,** 363–403.

Lett, C., J. Veitch, C. D. van der Lingen, and L. Hutchings, 2007: Assessment of an environmental barrier to the transport of ichthyoplankton from the southern to the northern Benguela ecosystems. *Mar. Ecol.,* **347,** 247–259.

Lutjeharms, J., 1996: The exchange of water between the south Indian and South Atlantic Oceans. *The South Atlantic: Past and Present Circulation,* G. Wefer et al., Eds., Springer-Verlag, 125–162.

——, and J. Meeuwis, 1987: The extent and variability of south-east Atlantic upwelling. *S. Afr. J. Mar. Sci.,* **5,** 51–62.

——, and P. Stockton, 1987: Kinematics of the upwelling front off southern Africa. *S. Afr. J. Mar. Sci.,* **5,** 35–49.

——, and R. van Ballegooyen, 1988: The retroflection of the Agulhas Current. *J. Phys. Oceanogr.,* **18,** 1570–1583.

——, F. Shillington, and C. M. Duncombe-Rae, 1991: Observations of extreme upwelling filaments in the southeast Atlantic Ocean. *Science,* **253,** 774–776.

——, D. Webb, B. de Cuevas, and S. Thompson, 1995: Large-scale modelling of the south-east Atlantic upwelling system. *S. Afr. J. Mar. Sci.,* **16,** 205–225.

Marchesiello, P., and P. Estrade, 2010: Upwelling limitation by coastal geostrophic convergence. *J. Mar. Res.,* in press.

——, J. McWilliams, and A. Shchepetkin, 2001: Open boundary conditions for long-term integration of regional oceanic models. *Ocean Modell.,* **3,** 1–20.

——, ——, and ——, 2003: Equilibrium structure and dynamics of the California Current system. *J. Phys. Oceanogr.,* **33,** 753–783.

——, L. Debreu, and X. Couvelard, 2009: Spurious diapycnal mixing in terrain-following coordinate models: The problem and a solution. *Ocean Modell.,* **26,** 156–169.

Matano, R., and E. Beier, 2003: A kinematic analysis of the Indian/Atlantic interocean exchange. *Deep-Sea Res.,* **50,** 229–249.

Mohrholz, V., M. Schmidt, J. Lutjeharms, and H.-C. John, 2001: The hydrography and dynamics of the Angola-Benguela frontal zone in April 1999. *S. Afr. J. Sci.,* **97,** 199–208.

Monteiro, P. M. S., and A. K. van der Plas, 2006: Low oxygen water (LOW) variability in the Benguela system: Key processes and forcing scales relative to forecasting. *Large Mar. Ecosyst.,* **14,** 71–90.

——, ——, J.-L. Mélice, and P. Florenchie, 2008: Interannual hypoxia variability in a coastal upwelling system: Ocean–shelf exchange, climate and ecosystem-state implications. *Deep-Sea Res. I,* **55,** 435–450.

Narimousa, S., and T. Maxworthy, 1986: Coastal upwelling on a sloping bottom: The formation of plumes, jets and pinched-off cyclones. *J. Fluid Mech.,* **176,** 169–190.

Nelson, G., and L. Hutchings, 1983: The Benguela upwelling area. *Prog. Oceanogr.,* **12,** 333–356.

Peffley, M., and J. O'Brien, 1976: A three-dimensional simulation of coastal upwelling off Oregon. *J. Phys. Oceanogr.,* **6,** 164–180.

Penven, P., 2000: A numerical study of the Southern Benguela circulation with an application to fish recruitment. Ph.D. thesis, University of Brest, 146 pp.

——, C. Roy, A. Colin de Verdiere, and J. Largier, 2000: Simulation of a coastal jet retention process using a barotropic model. *Oceanol. Acta,* **23,** 615–634.

——, ——, G. Brundrit, A. Colin de Verdiere, P. Freon, A. Johnson, J. Lutjeharms, and F. Shillington, 2001: A regional hydrodynamic model of upwelling in the southern Benguela. *S. Afr. J. Sci.,* **97,** 472–475.

——, V. Echevin, J. Pasapera, F. Colas, and J. Tam, 2005: Average circulation, seasonal cycle, and mesoscale dynamics of the Peru Current system: A modeling approach. *J. Geophys. Res.,* **110,** C10021, doi:10.1029/2005JC0029452.

——, N. Chang, and F. Shillington, 2006a: Modelling the Agulhas Current using SAfE (Southern African Experiment). *Geophys. Res. Abstr.,* **8,** 4225.

——, L. Debreu, P. Marchesiello, and J. McWilliams, 2006b: Evaluation and application of the ROMS 1-way embedding procedure to the central California upwelling system. *Ocean Modell.,* **12,** 157–187.

——, J. R. E. Lutjeharms, and P. Florenchie, 2006c: Madagascar: A pacemaker for the Agulhas Current? *Geophys. Res. Lett.,* **33,** L17609, doi:10.1029/2006GL026854.

——, P. Marchesiello, L. Debreu, and J. Lefèvre, 2007: Software tools for pre- and post-processing of oceanic regional simulations. *Environ. Model. Software,* **23,** 660–662, doi:10.1016/j.envsoft.2007.07.004.

Peterson, R., and L. Stramma, 1991: Upper-level circulation in the South Atlantic. *Prog. Oceanogr.,* **26,** 1–73.

Preston-Whyte, R. A., and P. D. Tyson, 1993: *The Atmosphere and Weather of Southern Africa*. Oxford University Press, 207–249.

Reid, J., 1989: Geostrophic circulation of the South Atlantic Ocean. *Prog. Oceanogr.,* **23,** 149–244.

Rio, M.-H., and F. Hernandez, 2004: A mean dynamic topography computed over the world ocean from altimetry, in situ measurements, and a geoid model. *J. Geophys. Res.,* **109,** C12032, doi:10.1029/2003JC002226.

Shannon, L., 1985: The Benguela ecosystem. Part 1: Physical features and processes. *Oceanographic and Marine Biology: An Annual Review,* M. Barnes, Ed., Vol. 23, 105–182.

——, and D. Hunter, 1988: Notes on Antarctic intermediate water around Southern Africa. *S. Afr. J. Mar. Sci.,* **6,** 107–117.

——, and G. Nelson, 1996: The Benguela: Large-scale features and processes and system variability. *The South Atlantic: Present and Past Circulation,* G. Wefer, Ed., Springer, 163–210.

——, J. Agenbag, and M. Buys, 1987: Large- and meso-scale features of the Angola-Benguela Front. *S. Afr. J. Mar. Sci.,* **5,** 11–34.

Shchepetkin, A. F., and J. C. McWilliams, 1998: Quasi-monotone advection schemes based on explicit locally adaptive dissipation. *Mon. Wea. Rev.,* **126,** 1541–1580.

——, and ——, 2003: A method for computing horizontal pressure-gradient force in an oceanic model with a nonaligned vertical coordinate. *J. Geophys. Res.,* **108,** 3090, doi:10.1029/2001JC001047.

——, and ——, 2005: The Regional Oceanic Modeling System (ROMS): A split-explicit, free-surface, topography-following-coordinate oceanic model. *Ocean Modell.,* **9,** 347–404.

Shillington, F., and L. Nykjaer, 2001: Environmental conditions and fluctuations in distribution in small pelagic fish stocks (ENVIFISH) 1998–2001. Small Pelagic Fishes and Climate Change Programme, GLOBEC Rep. 16, 79–80.

——, W. Peterson, L. Hutchings, T. Probyn, H. Waldron, and J. Agenbag, 1990: A cool upwelling filament off Namibia, southwest Africa: Preliminary measurements of physical and biological features. *Deep-Sea Res.,* **37,** 1753–1772.

Skogen, M., 1999: Numerical modelling of the Benguela system. Some preliminary results. *S. Afr. J. Mar. Sci.,* **21,** 235–249.

Speich, S., J. R. E. Lutjeharms, P. Penven, and B. Blanke, 2006: Role of bathymetry in Agulhas Current configuration and behaviour. *Geophys. Res. Lett.,* **33,** L23611, doi:10.1029/2006GL027157.

Stenevik, E., H. Verheye, M. Lipinski, M. Ostrowski, and T. Stromme, 2008: Drift routes of cape hake eggs and larvae in the southern Benguela Current system. *J. Plankton Res.,* **30,** 1147–1156.

Strub, P. T., F. A. Shillington, C. James, and S. J. Weeks, 1998: Satellite comparison of the seasonal circulation in the Benguela and California current systems. *S. Afr. J. Mar. Sci.,* **19,** 99–112.

Veitch, J., P. Florenchie, and F. Shillington, 2006: Seasonal and interannual fluctuations of the Angola-Benguela frontal zone (ABFZ) using 4.5 km resolution satellite imagery from 1982 to 1999. *Int. J. Remote Sens.,* **27,** 987–998.

——, P. Penven, and F. Shillington, 2008: The Benguela: A laboratory for comparative modeling studies. *Prog. Oceanogr.,* **83,** 296–302, doi:10.1016/j.pocean.2009.07.008.